Supporting information

Heterocycles for direct air capture and MOFs prepared from CO_2 utilization

Jingcheng Du,[1] Linghao Liu,[1] Qian Sun,[1] Ziye Song,[1] Ayan Yao,[1]Ji Ma,[1]Tai-Shung Chung,[2,3] * Wei Xu,[4]Hongjun Zhang,[4] Jiangtao Liu [1, *]

[1]Department of Environmental Science and Engineering, University of Science and Technology of China, Hefei, China, 230052

[2]Department of Chemical and Biomolecular Engineering, National University of Singapore, 117576, Singapore

[3]Graduate Institute of Applied Science and Technology, National Taiwan University of Science and Technology, Taipei, Taiwan, 10607

[4]State Key Laboratory of Particle Detection and Electronics, University of Science and Technology of China, Hefei, China, 230052

1. Experimental

1.1 Materials

All chemicals and solvents used in the syntheses were of reagent grade and used without any further purification. Zinc nitrate hexahydrate ($Zn(NO_3)_2 \cdot 6H_2O$, 99%) was of analytical grade and ordered from Shanghai Aladdin Biochemical Technology Co., Ltd.

(Shanghai, China). Zinc acetate dihydrate ($C_4H_6O_4Zn \cdot 2H_2O$, 99%), zinc sulfate heptahydrate ($ZnSO_4 \cdot 7H_2O$, 99.5%), N, N-dimethylformamide (C_3H_7NO, 99.5%), acetonitrile (C_2H_3N, 99.5%), isopropanol (C_3H_8O, 99.7%), dichloromethane (CH_2Cl_2, 99.5%), potassium carbonate (K_2CO_3, 99.0%), hydrochloric acid (HCl, 36.0-38.0%), and toluene (C_7H_8, 99.5%) were of analytical grade and purchased from Sinopharm Chemical Reagent Co., Ltd. (Shanghai, China). Piperazine ($C_4H_{10}N_2$, 97%) and 1,4,8,11-tetraazacyclotetradecane ($C_{10}H_{24}N_4$, 98%) were obtained from Shanghai Tensus Biotech Co., Ltd. (Shanghai, China). 1,4,7-Triazacyclononane ($C_6H_{15}N_3$, 98%) was received from Shanghai Macklin Biochemical Co., Ltd. (Shanghai, China). High purity H_2 (≥99.999%) CO_2 (≥99.999%), N_2 (≥99.999%) and CH_4 (≥99.999%) were purchased from Nanjing Shangyuan Industrial Gas Factory. Air source was acquired from Nanjing Special Gas Co. Ltd. 5,5',6,6'-Tetrahydroxy-3,3,3',3'-tetramethyl-1,1'-spirobisindane (TTSBI, 97%, Alfa Aesar), 2,3,5,6-Tetrafluoroterephthalonitrile (TFTPN, 99%, Sigma-Aldrich) was purified via sublimation.

1.2 DAC experiments

First, 10 mL MeCN and 1 mmol HC_4-N_2 were placed in a round-bottom flask and homogenized by a magnetic stirrer at 200 r/min. Then, the round-bottomed flask was loaded into the DAC testing system. The nondispersive infrared CO_2 meter, for detecting CO_2 concentration in the downstream of the reactor, was turned on. The air source was turned on, and the flow rate was adjusted to 60 mL min^{-1} for the DAC experiments.

1.3 Fabrication of HC_x-N_y-CO_2-Zn MOFs

1.3.1 Synthesis of HC_4-N_2-CO_2

The synthesis strategy of HC_x-N_y-CO_2 powders was carried out with slight modifications based on the previous literature [S1]. The specific preparation method was as follows: 0.75 mmol (51.68 mg) piperazine (HC_4-N_2) was dissolved in 20 mL IPA and ultrasonicated for 10 minutes in a 50 mL round-bottom flask filled with an agitator and rubber stopper. A clear and transparent colorless solution was obtained. N_2 was added and swept for 10 minutes to remove air in the aqueous solvent and round-bottom flask. Rapidly, CO_2 was introduced into the bottom of the round-bottom flask using a catheter at room temperature and pressure, accompanied by bubbles in the solvent. In this process, continuous magnetic stirring (960 r/min) made the distribution of starting materials and CO_2 more uniform. After 1 minute, a white precipitate was produced. As the reaction proceed, more CO_2 reacted with the secondary amine groups of HC_4-N_2, resulting in an increasing number of products until the reaction was completed after 3 hours. The white precipitate was centrifugally washed with isopropanol 3 times and dried in a vacuum drying oven at 25 °C for 10 h. Finally, a white powder was obtained by grinding.

1.3.2 Synthesis of HC_6-N_3-CO_2

The HC_6-N_3-CO_2 powder synthesis strategy was similar to that of HC_4-N_2-CO_2 with slight modifications. The specific preparation method was as follows: First, 0.75 mmol 96.91 mg 1,4,7-triazacyclononane (HC_6-N_3) was dissolved in 20 mL MeCN organic solvent. As reported in the previous literature [S2], MeCN is more conducive to the dissolution of CO_2 due to the presence of nitrogenous groups with a strong affinity for

67 CO_2 and is more conducive to realizing a high yield. A clear and transparent colorless
68 solution was obtained in a 50 mL round-bottom flask with a rubber stopper and agitator
69 for 10 min by ultrasound. Thereafter, N_2 was injected for 10 minutes to remove air from
70 the solvent and round-bottomed flask. Promptly, CO_2 was introduced into the bottom
71 of the round-bottomed flask using a catheter at room temperature and pressure,
72 accompanied by bubbles in the solvent. During this process, magnetic stirring (960
73 r/min) was carried out continuously to make the distribution of starting materials and
74 CO_2 more uniform. A white precipitate was generated after 5 s, indicating that the
75 reactive activation of HC_6-N_3 was higher than that of HC_4-N_2 due to the special
76 chemical structure. As the reaction progressed, more CO_2 reacted with the secondary
77 amine group of HC_6-N_3, resulting in an increasing number of products until the reaction
78 ended 2 hours later. The white precipitate was washed 3 times by centrifugation with
79 the MeCN solvent and dried in a vacuum drying oven for 10 hours. After grinding,
80 white powders were also obtained.

81 **1.3.3 Synthesis of HC_{10}-N_4-CO_2**

82 The synthesis strategy of HC_{10}-N_4-CO_2 powders was similar to that of HC_4-N_2-CO_2
83 with only slight modifications. The specific preparation method was as follows: First,
84 1.50 mmol 300.50 mg needle-like 1,4,8,11-tetraazacyclotetradecane (HC_{10}-N_4) as the
85 starting material was dissolved in a 30 mL MeCN organic solvent of 30 mL. A clear
86 and transparent colorless solution was obtained in a 50 mL round-bottom flask with a
87 rubber stopper and agitator for 10 min by ultrasound. Similarly, N_2 was injected for 10
88 minutes to remove air from the solvent and round-bottomed flask. Rapidly, CO_2 was

introduced into the bottom of the round-bottomed flask using a catheter at room temperature and pressure, accompanied by bubbles in the solvent. During this process, magnetic stirring (960 r/min) was carried out continuously to make the distribution of starting materials and CO_2 more uniform. After 30 min, a white precipitate was produced, indicating that the reactive activation of HC_{10}-N_4 was lower than that of HC_4-N_2 and HC_6-N_3 due to the more complex chemical structure. As the reaction progressed, more CO_2 reacted with the secondary amine groups of HC_{10}-N_4, resulting in an increasing number of products until the reaction ended after 5 hours. The white precipitate was washed 3 times by centrifugation with MeCN and dried in a vacuum drying oven for 10 h. After grinding, white powders were also obtained.

1.3.4 Synthesis of HC_4-N_2-CO_2-ZnX (X=OAC^-, NO_3^-, SO_4^{2-})

The synthesis strategy of HC_4-N_2-CO_2-ZnX powders was carried out as follows: Initially, 0.8 mmol 175.6 mg $Zn(OAC)_2 \cdot 2H_2O$ [0.8 mmol 237.99 mg $Zn(NO_3)_2 \cdot 6H_2O$ or 0.8 mmol 230.05 mg $ZnSO_4 \cdot 7H_2O$] and 0.75 mmol (51.68 mg) HC_4-N_2 were dissolved in 20 mL N,N-dimethylformamide (DMF) and 20 mL IPA solvent, respectively. The clear and transparent colorless solution was obtained by ultrasound for 10 min. N_2 bubbling was carried out and purged for 10 min to remove the air in the metal solution and round-bottom flask. $Zn(OAC)_2 \cdot 2H_2O$, $Zn(NO_3)_2 \cdot 6H_2O$ or $ZnSO_4 \cdot 7H_2O$ and HC_4-N_2 solution were placed in a 100 mL round-bottom flask filled with an agitator and rubber stopper. Promptly, CO_2 was introduced into the bottom of the round-bottom flask using a catheter at room temperature and pressure, accompanied by bubbles in the solvent. During this process, magnetic stirring (960 r/min) was carried

111 out continuously to make the distribution of starting materials and CO_2 more uniform.
112 After 10 s, a white precipitate occurred. As the reaction proceeded, CO_2 reacted with
113 the secondary amine groups of HC_4-N_2 to form HC_4-N_2-CO_2, which acted as the ligands
114 of the MOFs. Ultimately, the resulting ligands reacted with six-coordinated zinc
115 clusters to form Zn-MOFs. As the reaction progressed, an increasing number of white
116 products were produced until the reaction was over three hours later. The final white
117 precipitates, HC_4-N_2-CO_2-$Zn(OAC)_2$, HC_4-N_2-CO_2-$Zn(NO_3)_2$, and HC_4-N_2-CO_2-
118 $ZnSO_4$, were centrifugally washed with DMF and IPA 3 times and dried in a vacuum
119 oven for 10 hours. The white powders were ground, sealed and preserved under
120 vacuum.

121 **1.3.5 Synthesis of HC_6-N_3-CO_2-ZnY (Y=OAC^-, NO_3^-)**

122 The synthesis strategy of HC_6-N_3-CO_2-ZnY powders was similar to that of HC_4-N_2-
123 CO_2-ZnX. The specific method was carried out as follows: First, 0.9 mmol 197.56 mg
124 $Zn(OAC)_2 \cdot 2H_2O$ [0.9 mmol 267.74 mg $Zn(NO_3)_2 \cdot 6H_2O$] and 0.75 mmol 96.91 mg
125 HC_6-N_3 were dissolved in 20 mL DMF and 20 mL MeCN, respectively. Thereafter, the
126 solutions were fully dissolved by ultrasound for 10 min to obtain clear and transparent
127 colorless solutions. A N_2 bubble was added and purged for 10 minutes to remove the
128 air in the solvent. The $Zn(OAC)_2 \cdot 2H_2O$ [$Zn(NO_3)_2 \cdot 6H_2O$] and HC_6-N_3 solutions were
129 placed in a 100 mL round-bottom flask with a rubber stopper filled with an agitator.
130 Rapidly, CO_2 was introduced into the bottom of the round-bottom flask using a catheter
131 at room temperature and pressure, accompanied by bubbles in the solvent and round-
132 bottomed flask. A white precipitate was formed immediately with the entry of CO_2.

133 During this process, magnetic stirring (960 r/min) was carried out continuously to make
134 the distribution of starting materials and the CO_2 system more uniform. In this reaction
135 system, CO_2 reacted with the secondary amine groups of HC_6-N_3 to form HC_6-N_3-CO_2
136 as the ligands of MOFs. Furthermore, the resulting ligands reacted with six-coordinated
137 zinc clusters to form Zn-MOFs. As the reaction progressed, an increasing number of
138 white products was produced until the reaction was conducted over 2 hours. The white
139 precipitate was centrifugally washed with DMF and MeCN 3 times and dried in a
140 vacuum oven for 10 h. Fine HC_6-N_3-CO_2-$Zn(OAC)_2$ and HC_6-N_3-CO_2-$ZnNO_3$ white
141 powders were obtained by grinding, which were sealed and stored in vacuum for later
142 use.

143 **1.3.6 Synthesis of HC_{10}-N_4-CO_2-$Zn(OAC)_2$**

144 The synthesis strategy of HC_{10}-N_4-CO_2-$Zn(OAC)_2$ powders was as follows: 1.5 mmol
145 329.27 mg $Zn(OAC)_2 \cdot 2H_2O$ and a certain amount of HC_{10}-N_4-CO_2 powder were
146 dissolved in 20 mL DMF and 20 mL IPA, respectively. Two clear and transparent
147 colorless solutions were obtained by ultrasound for 10 min. N_2 was added and purged
148 for 10 min to remove the air in the solvents and round-bottomed flask. The
149 $Zn(OAC)_2 \cdot 2H_2O$ and HC_{10}-N_4-CO_2 solutions were placed in a 100 mL round-bottom
150 flask with a rubber stopper filled with an agitator. Rapidly, CO_2 was introduced into the
151 bottom of the round-bottom flask using a catheter at room temperature and pressure,
152 accompanied by bubbles in the solvent. During this process, magnetic stirring (960
153 r/min) was carried out continuously to make the distribution of starting materials and
154 CO_2 more uniform. In the process, HC_{10}-N_4-CO_2, as the ligand, reacted with six-

155 coordinated zinc clusters to form Zn-MOFs. After 6 hours of reaction, the liquid was
156 heated to 80 °C to precipitate the crystal powders. The white HC_{10}-N_4-CO_2-$Zn(OAC)_2$
157 powders obtained by grinding were sealed and stored in vacuum for later use.
158

159 **1.4 Fabrication of PIM-1-based mixed-matrix membranes**

160 **1.4.1 TTSBI and TFTPN purification**

161 5,5',6,6'-Tetrahydroxy-3,3,3',3'-tetramethyl-1,1'-spirobisindane (TTSBI) powders
162 (26 g) and methanol (MeOH, 140 g) were mixed into a conical flask with a stirrer. Then
163 the bottle was placed on a 65 °C heater and stirred for 4 hours. After finishing above
164 process, the heater was turned off. Dichloromethane (DCM, 40 g) was added into the
165 bottle. After 30 min, the bottle was placed in a refrigerator for 2 hours. Finally, the
166 mixture was filtered and rinsed by methanol to obtain purified TTSBI. 2,3,5,6-
167 Tetrafluoroterephthalonitrile (TFTPN) was purified via sublimation using a homemade
168 equipment.

169 **1.4.2 synthesis of PIM-1 powders**

170 The typical procedure for synthesis of PIM-1 was carried out as follows: TTSBI (1.55
171 g, 4.5 mmol), TFTPN (0.91 g, 4.5 mmol), and K_2CO_3 (2.51 g, 18.0 mmol), and freshly
172 distilled DMF (30 mL) were added to a 50 mL round-bottomed flask equipped with a
173 magnetic stirrer, a nitrogen inlet and a reflux condenser. The system was purged with
174 N_2 and then the N_2 inlet was removed and the mixture was placed on a hot stirring plate
175 and stirred at 600 rpm. The mixture was heated to 100 °C and 1.0 mL toluene was added
176 to the system and maintained at this temperature for 24 h to ensure high molecular

177 polymers. With the polymerization process, a yellowish suspension was gradually
178 obtained. Then the solution was cooled down to room temperature and carefully poured
179 into 300 mL deionized water with a vigorously stirred magnetic stirrer to yield a
180 powder-like precipitate. The residual K_2CO_3 was removed by adding 1M HCl until CO_2
181 evolution stopped and pH was about 5. The recovered precipitate was filtered, then
182 washed thoroughly with deionized water for several times until pH was about 7. After
183 that, the orange precipitate was washed several times with methanol at 60 °C to remove
184 the organic solvent. Finally, the orange solid dried at 80 °C under high vacuum for 12
185 h.

186 **1.4.3 Fabrication of mixed-matrix membranes**

187 PIM-1-based MMMs were fabricated by a priming process. PIM-1 (0.2 g) was
188 dissolved in CH_2Cl_2 (9.8 g) to obtain a 2 wt% solution. MOF nanoparticles (2 mg) were
189 dispersed in the above PIM-1 solution and violently stirred for 12 h to obtain a uniform
190 dispersion. Finally, the casting solution was poured into a homemade mold with a glass
191 lid to slow down its evaporation rate, and the evaporation process was controlled for 12
192 h. The obtained membranes were dried for 12 h before the tests.

193 **1.4 Separation performance tests**

194 Separation performance tests were carried out by using a home-made gas permeability
195 analyzer at 298 K. The prepared membrane with an effective area of 0.28 cm^2 was
196 sealed and placed in the permeation cell by using an O-ring. Pure gas was used as the
197 feed gas. The inlet pressure was regulated through an upstream vacuum pump, while
198 the permeate side was vacuum-treated. Finally, the feed gas would pass through the 1 %

199 HC_6-N_3-CO_2-$Zn(NO)_3$ mixed matrix membranes into the permeate side. Gas
200 permeability (P) was calculated based on the membrane thickness, permeate time,
201 permeate volume, transmembrane pressure, and effective membrane area. Selectivity
202 (α) was calculated by the permeability of different gases (Pi and Pj):

203 $$\alpha = P_i/P_j$$

204 **1.5 Characterizations of HC_x-N_y-CO_2-Zn MOFs**

205 Powder X-ray diffraction (PXRD, Bruker D8 Advance) was employed to investigate
206 the crystalline structure of MOFs powders in a 2θ range of 5-50° utilizing Cu K-α
207 (λ=1.54 Å) as the X-ray radiation source. The chemical structures of the synthesized
208 HC_x-N_y-CO_2-Zn MOFs were identified using a Bruker Tensor II Fourier transform
209 infrared spectrometer with a wavenumber range of 400-4000 cm^{-1}. X-ray photoelectron
210 spectroscopy (XPS, Kratos AXIS SUPRA+) equipped with an Al Kα X-ray source
211 (1486.6 eV) was used to analyze the chemical structure and element composition of
212 MOFs. The morphology of the starting material and MOFs were further determined by
213 field emission scanning electron microscopy (FESEM, Quanta FEG 250). The
214 dispersion of samples was of great importance for SEM characterizations to obtain the
215 desired morphology. A variety of MOFs powders were uniformly dispersed by
216 ultrasonication for a certain time using different organic solvents before being dripped
217 onto a silicon wafer. All samples were sprayed with Pt/Pd alloy for 40 s using an auto
218 fine coater (208 HR, TED PELLA, INC.) and operating at a 20 mA current to enhance
219 the definition of SEM images. The thermal stability of different MOFs was evaluated
220 by a thermogravimetric analyzer (DTG-60H, SHIMADZU) in the temperature range of

25-800 °C with a heating ramp of 10 °C min^{-1} under a flowing N_2 atmosphere accompanying a flow of 50 mL min^{-1}. Field emission transmission electron microscopy images were obtained by a Talos F200X field emission transmission electron microscope at an accelerating voltage of 200 kV. Solvent-dispersed MOFs powders were loaded on copper grids for FE-TEM imaging. 1H NMR spectra were recorded on a Bruker Avance-600 (600 MHz) spectrometer. Chemical shifts were expressed in p.p.m. downfield from tetramethylsilane (TMS) at d δ= 0 p.p.m. and J values are given in Hz. The free volume size and distribution of the membranes were detected by positron annihilation lifetime spectroscopy (PALS). ^{22}Na isotope was employed as positron and g-ray (1275 keV) sources. The membrane samples were cut into pieces of 1 × 1 cm, and the thickness of each sample was stacked into a total thickness of approximately 1 mm.

Figure S1. Measurements of CO_2 concentration in the atmosphere by using a nondispersive infrared CO_2 meter (GMP252, Vaisala GmbH). The testing result was 408 ppm.

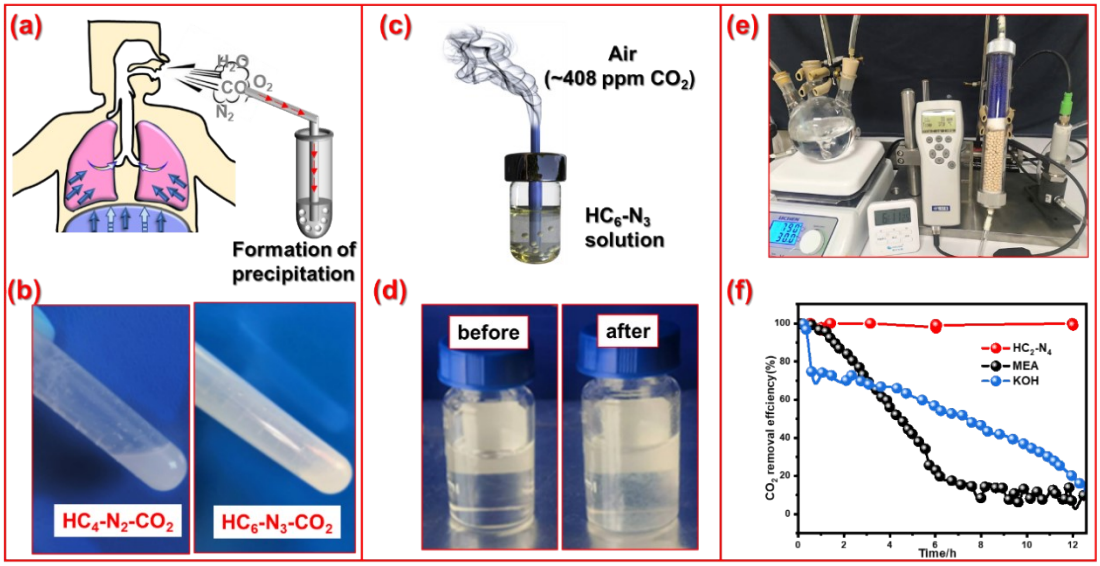

Figure S2. Visible DAC capacity analysis of HC_x-N_y. (a) Model diagram and (b) Digital images after HC_4-N_2 and HC_6-N_3 adsorbents absorbing CO_2 exhaled by a human body. (c) Model diagram of the experimental apparatus to capture CO_2 existing in the atmosphere. (d) Changes in the form of HC_6-N_3 before (left side) and after (right side) CO_2 captured in the atmosphere by comparing their digital images. (e) The CO_2 absorption testing system including air source, absorption reactor and detection system. (f) The CO_2 removal efficiency of HC_4-N_2, MEA, and KOH as a function of time.

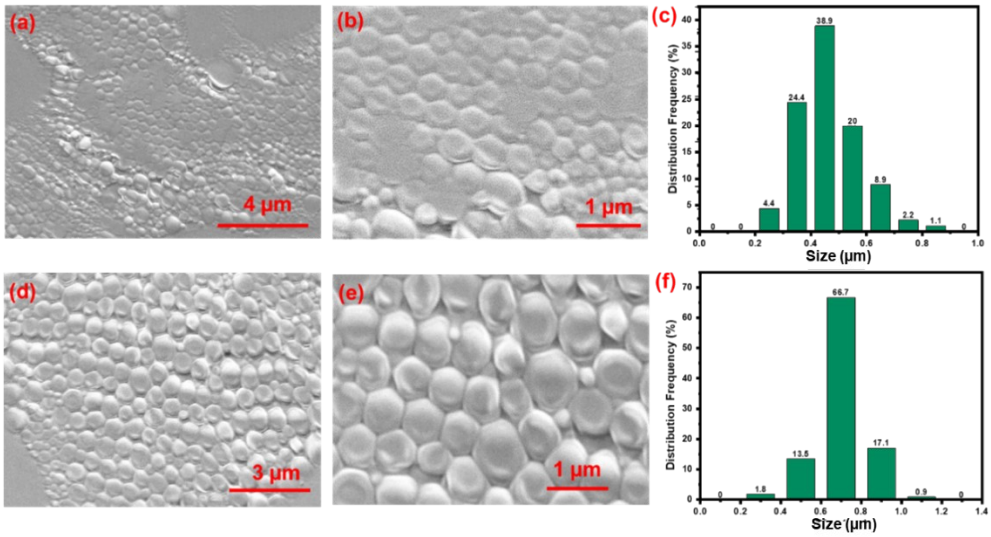

Figure S3. a, b, FESEM pictures and **C**, Size distribution of HC_4-N_2-CO_2 obtained in the atmosphere at different magnifications. d, e, FESEM pictures and f, Size distribution of HC_6-N_3-CO_2 obtained in the atmosphere at different magnifications. Size distributions in c and f were measured by a software.

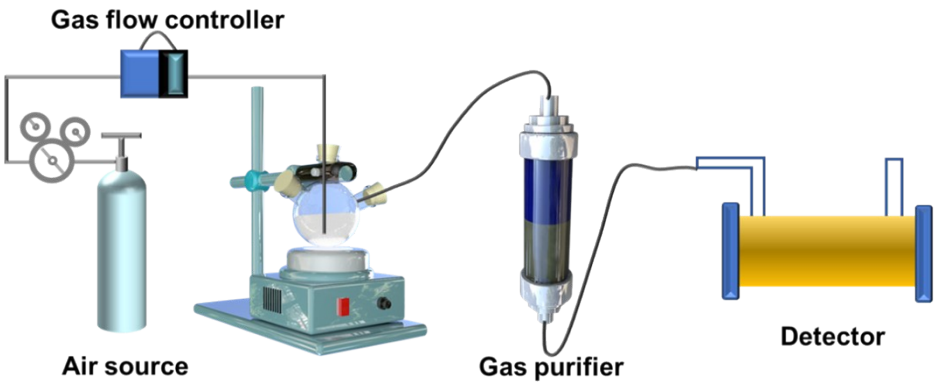

Figure S4. Schematic diagram of the CO_2 absorption testing system for the DAC process.

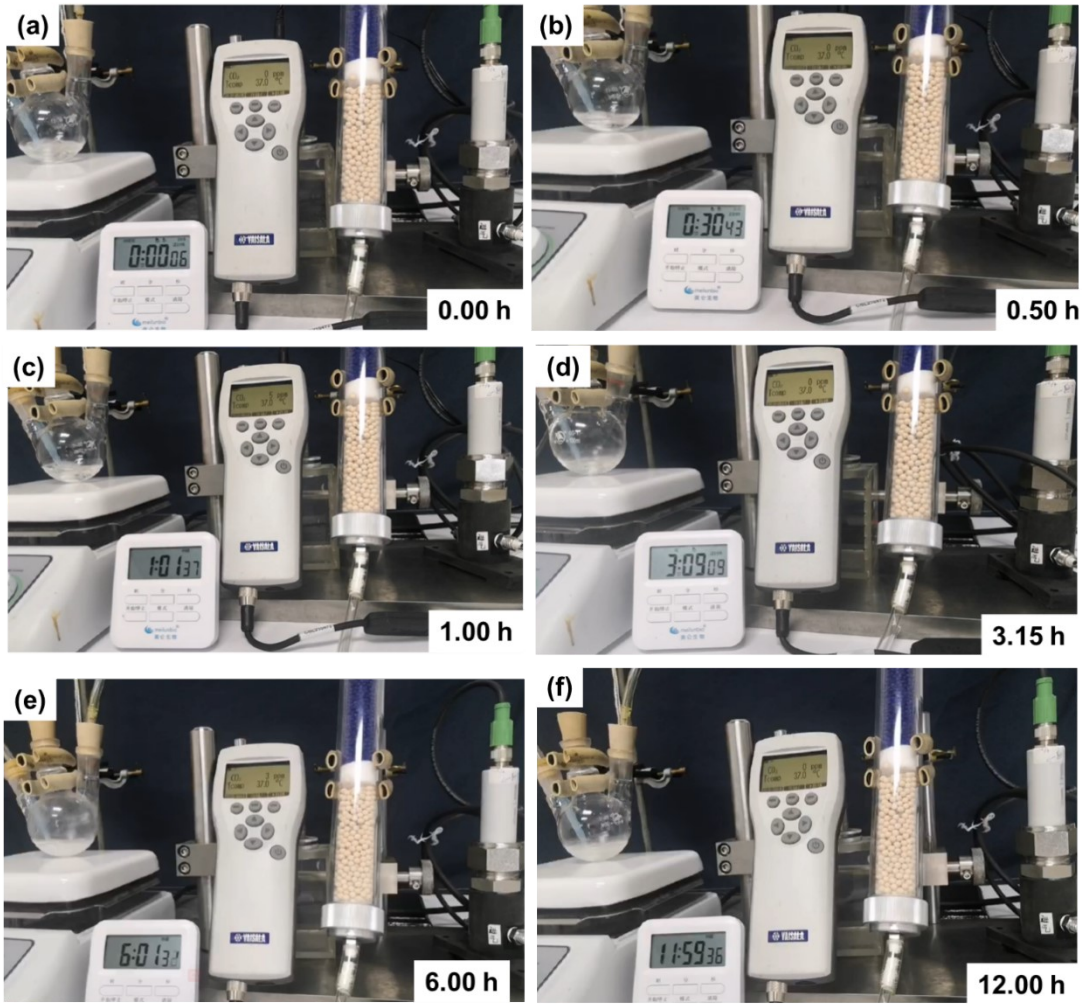

Figure S5. Photographs of the DAC process by using HC_4-N_2 in MeCN solutions under air sources. a, 0.00 h. b, 0.50 h. c, 1.00 h. d, 3.15 h. e, 6.00 h. f, 12.00 h. The downstream CO_2 concentration was monitored by using a nondispersive infrared CO_2 meter (GMP252, Vaisala GmbH).

Table S1. Comparison of CO_2 absorption performance of HC_x-N_y and other high performing adsorbents reported in the literature.

Material class	Material	P_{CO_2} (mbar)	T (°C)	g/kg	mol/Kg	Reference
Metal-organic frameworks	Te- Mg_2(dobpdc)	50	90	149.6	3.4	[S3]
	Mg_2(dobdc)	50	95	35.2	0.8	[S4]
	CALF-20	1200	20	179.1	4.1	[S5]
Zeolites	13X-IO10	900	30	46.2	1.1	[S6]
	13X-IO20	900	30	65.1	1.5	[S6]
	Na-GIS-3.0	200	25	162.8	3.7	[S7]
Ionic liquid	Graphene/IL	1000	25	374.0	8.5	[S8]
	[DEEA][Pent]	4000	60	10.6	0.2	[S9]
	P-DVB-AEImOH	1000	25	43.6	1.0	[S10]
Amine-decorated mesoporous solid	Mesoporous Silica	50	60	143.0	3.3	[S11]
	TEPA-MCM-41	129	75	140.8	3.2	[S12]
	SWIRL-TEPA	50	95	176.0	4.0	[S13]
		100	106	176.0	4.0	[S14]
Aza-fused π-conjugated networks	CTF-1-500	-	25	98.1	2.2	[S15]
	Bipy-CTF600	-	25	129.8	3.0	[S15]
	O-Doped CTFs	1000	24	211.2	4.8	[S16]
Amine adsorbent	IPDA	-	25	279.0	6.3	[S17]
	MEA	-	25	446.6	10.2	[S17]
HC_x-N_y	HC_4-N_2	100	25	1048.0	23.8	This work
	HC_6-N_3	100	25	1047.6	23.8	This work
	HC_{10}-N_4	100	25	898.0	20.4	This work

-: not available

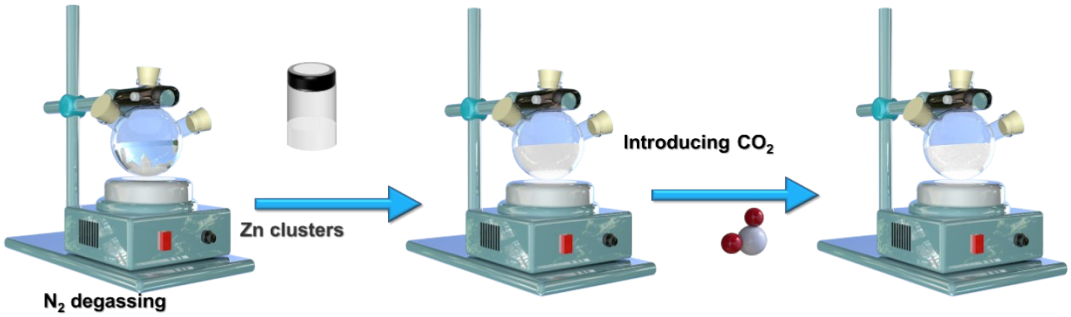

Figure S6. Diagram of the experimental device and the schematic diagram to prepare MOFs from CO_2, Zn clusters and HC_x-N_y.

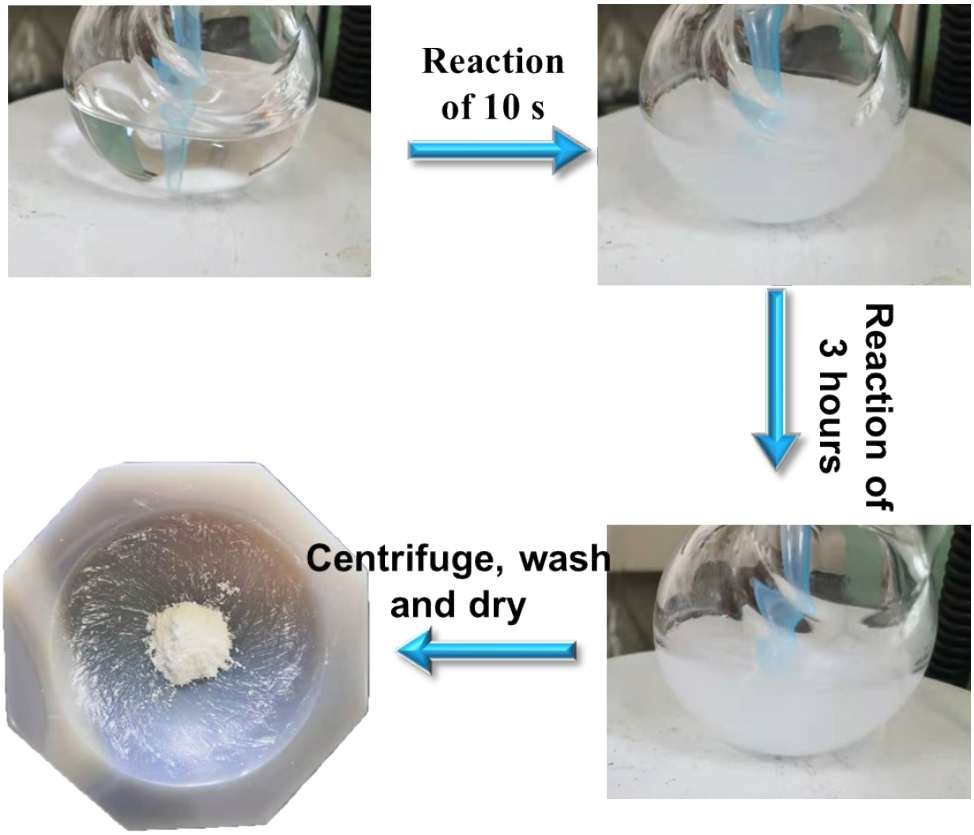

Figure S7. Flow diagrams of the preparation process for HC_4-N_2-CO_2-$Zn(OAC)_2$.

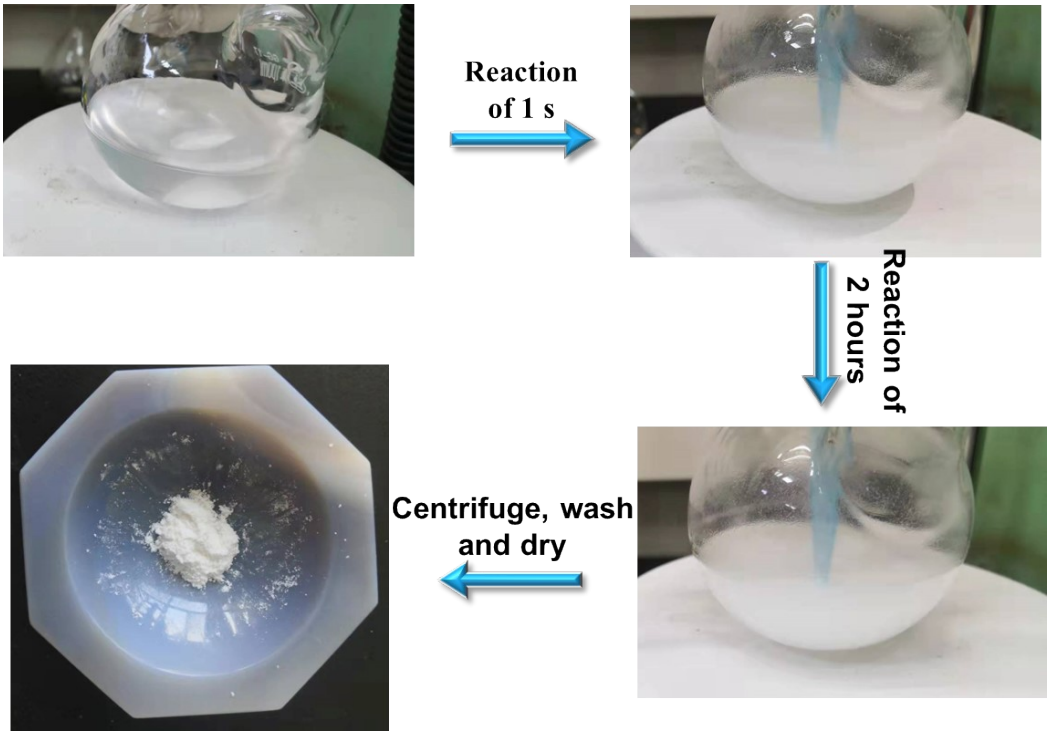

Figure S8. Flow diagrams of the preparation process for HC_6-N_3-CO_2-$Zn(OAC)_2$.

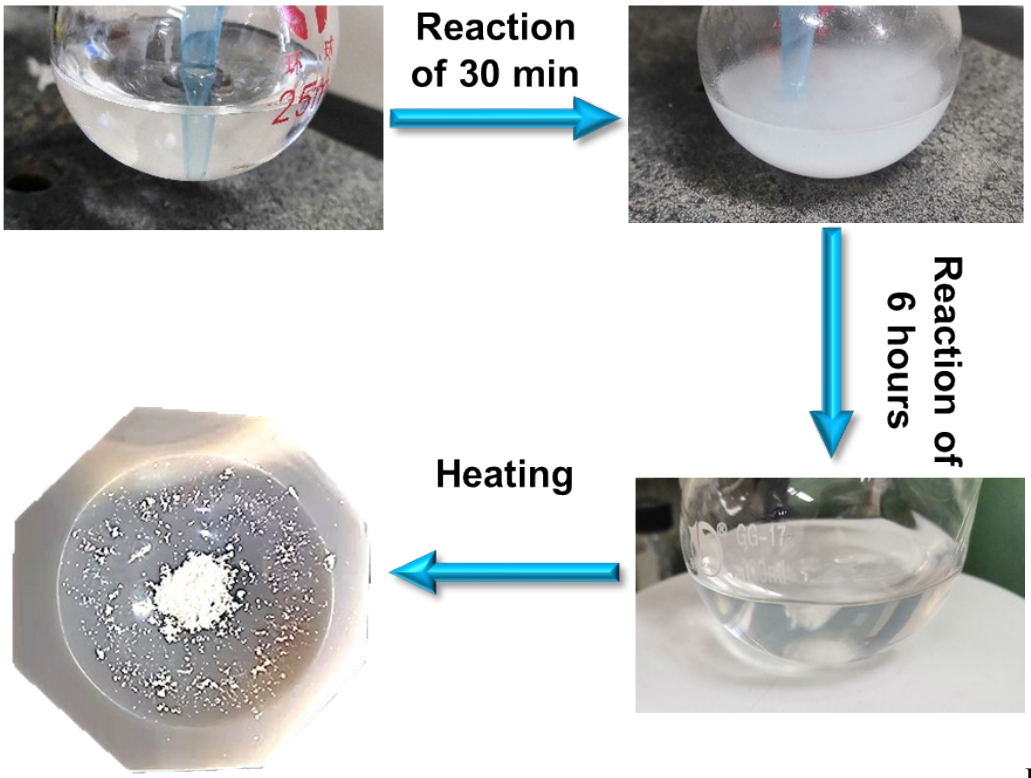

Figure S9. Flow diagrams of the preparation process for HC_{10}-N_4-CO_2-$Zn(OAC)_2$.

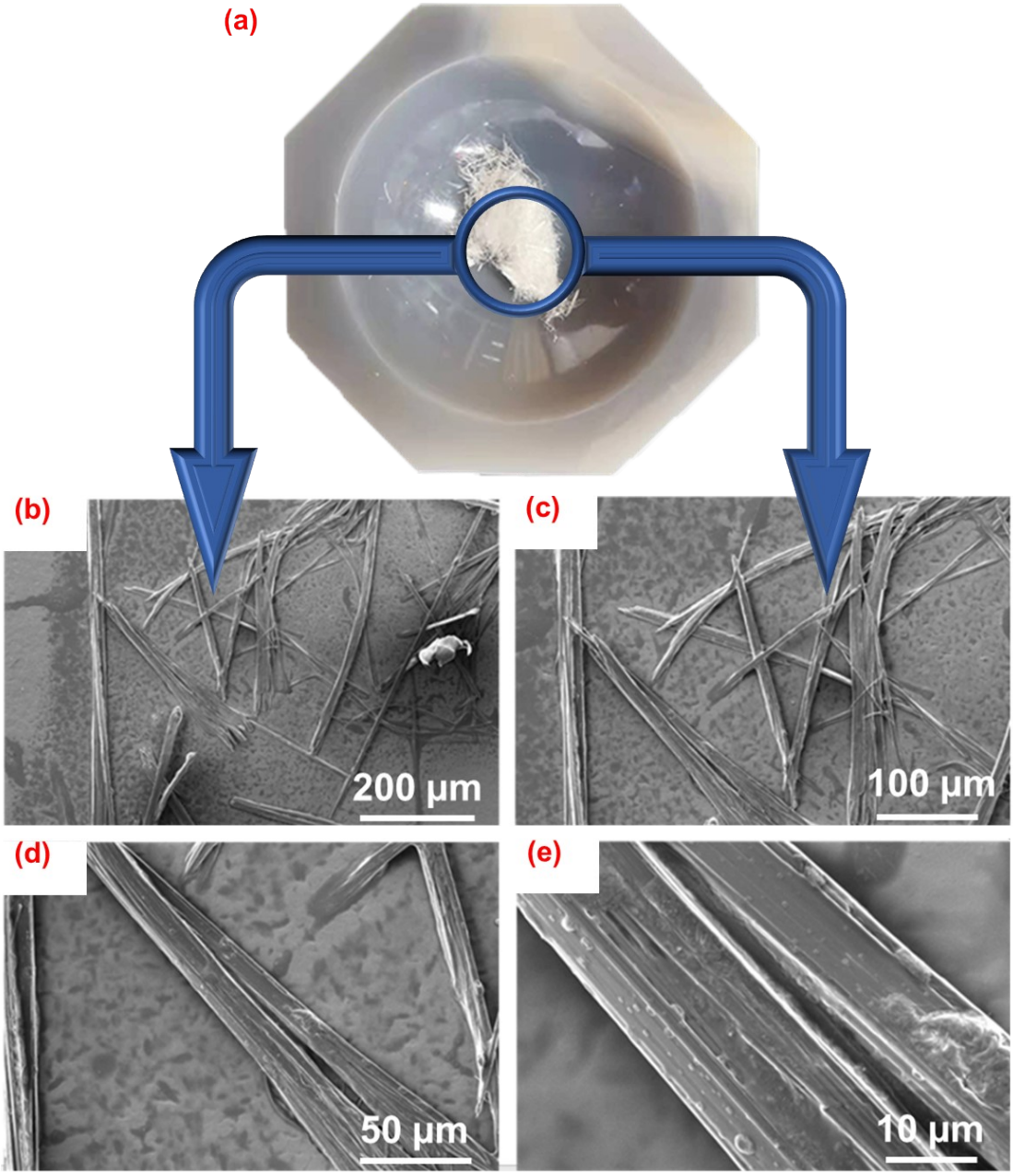

Figure S10. (a) Digital picture and (b-e) SEM images of HC_{10}-N_4 at different magnifications.

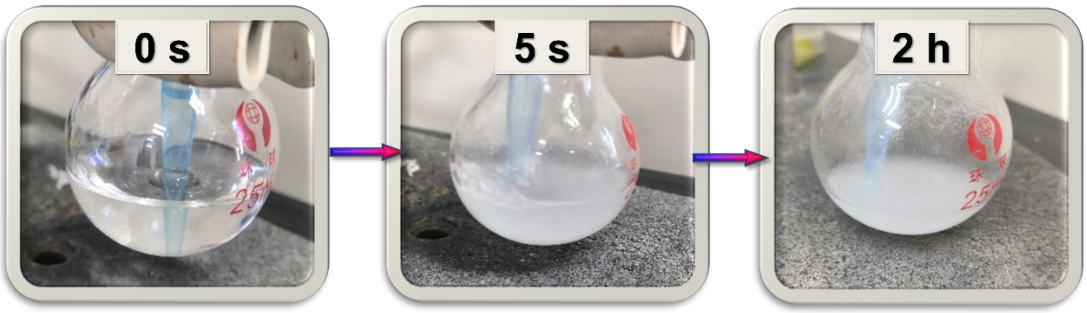

Figure S11. Digital images of reaction at reaction durations of 0 s, 5 s and 2 h in the HC_6-N_3 reaction system.

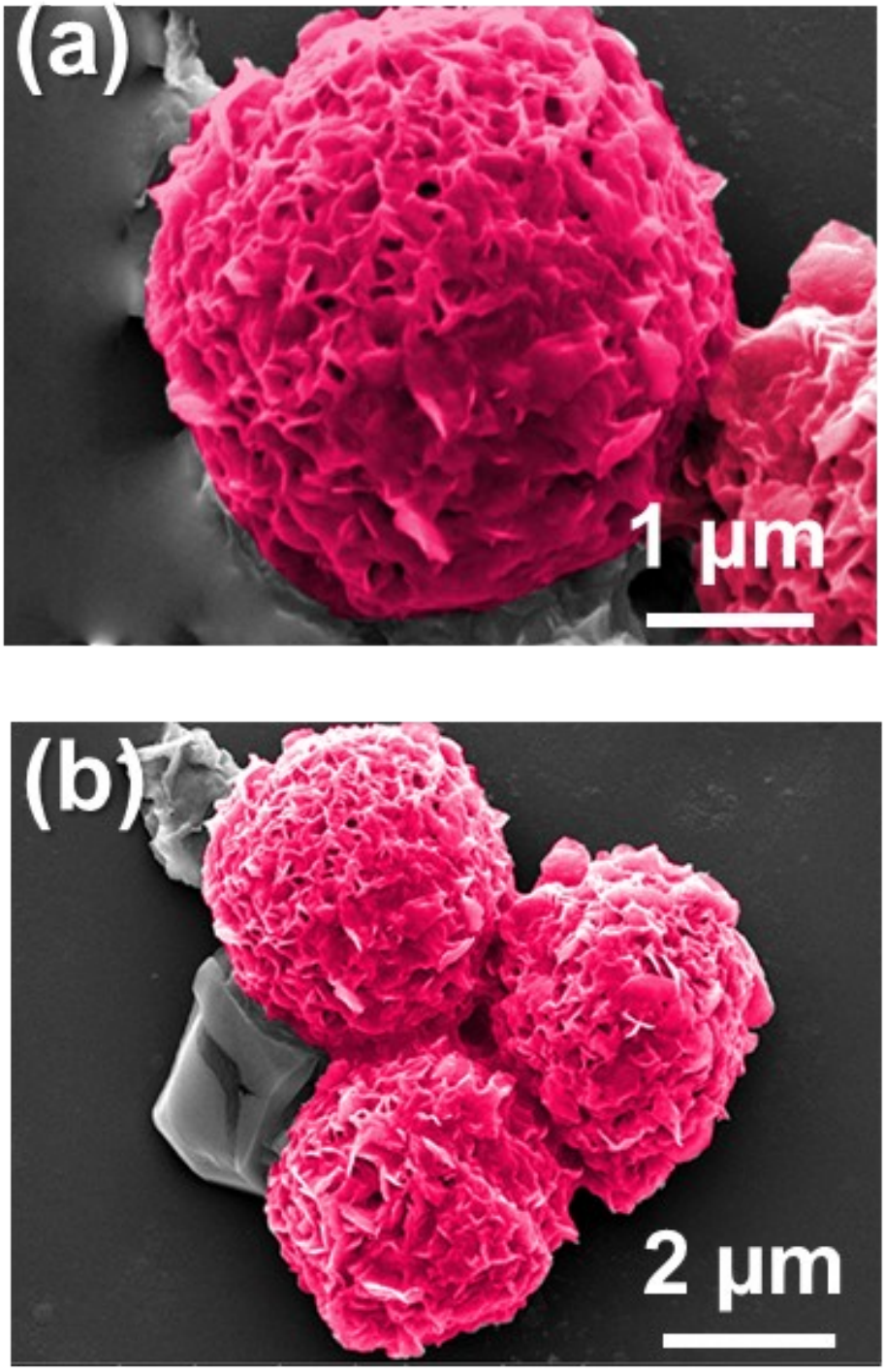

Figure S12. FESEM images of HC_4-N_2-CO_2-$ZnSO_4$. FESEM images were colored red for visual effect.

Table S2. A comparison of N content of different amines reported in the state-of-the-art literature.

Entry	Name	Structure	N content [a]	Reference
1	MEA	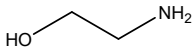	0.229	[S18]
2	IPDA	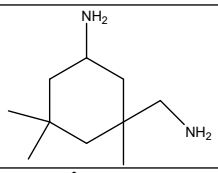	0.165	[S18]
3	Cyclohexane-1, 3-diamine	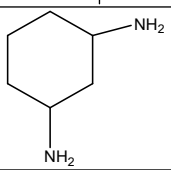	0.246	[S18]
4	DMAPA	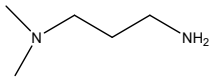	0.159	[S19]
5	Lysine	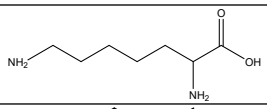	0.171	[S20]
6	2-methylpiperidine	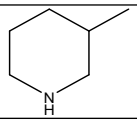	0.141	[S21]
7	MMEA	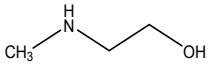	0.237	[S22]
8	DEAB	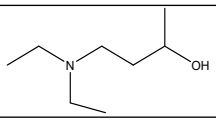	0.097	[S22]
9	MDEA	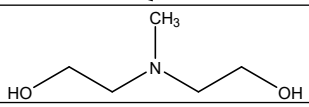	0.118	[S23]
10	HC_4-N_2	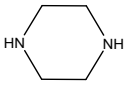	0.326	In this work
11	HC_6-N_3	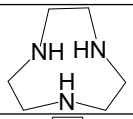	0.326	In this work
12	HC_{10}-N_4	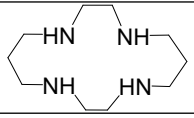	0.280	In this work

a represent the mass ratio of N to the molecular mass

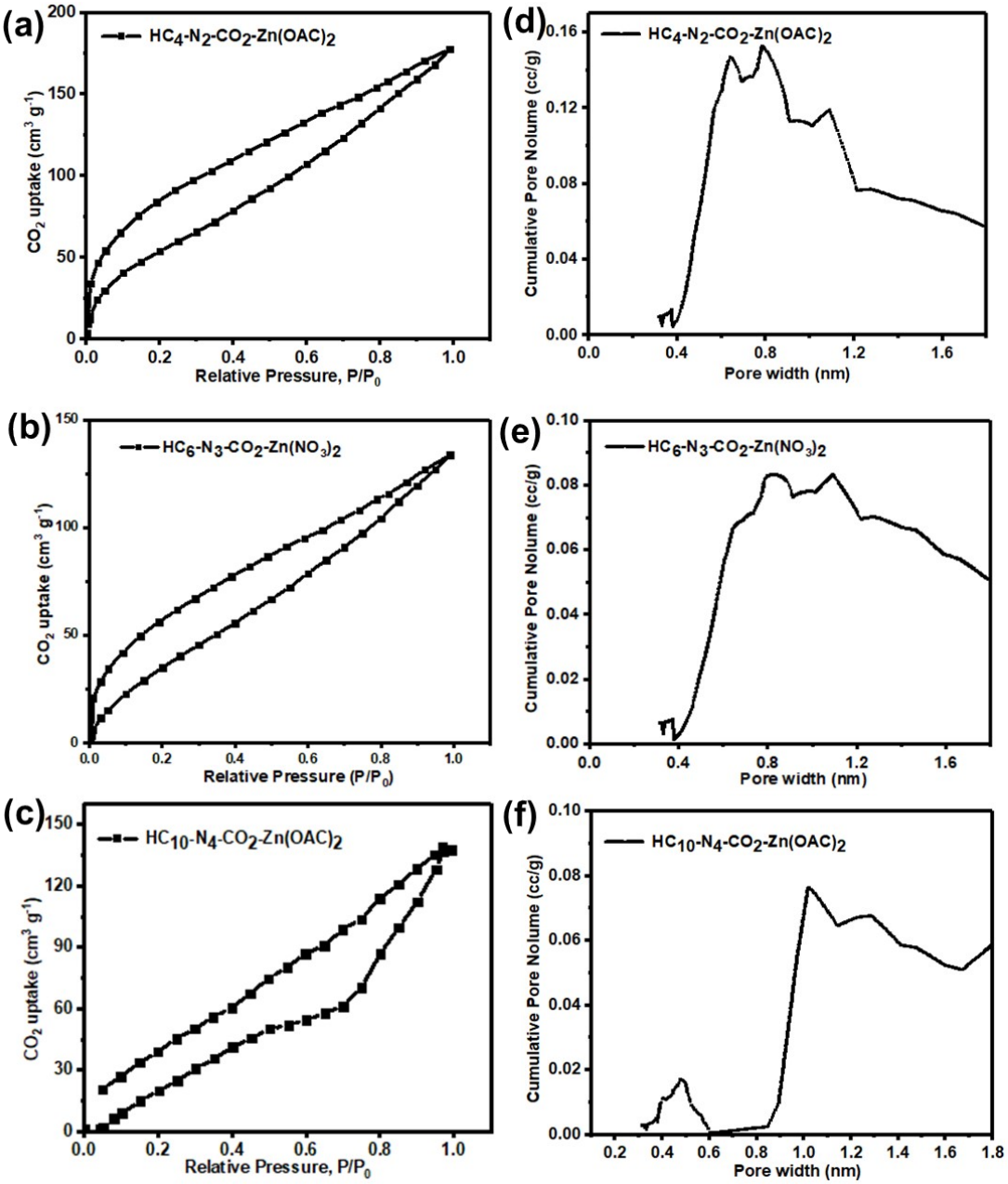

Figure S13 BET surface areas and pore sizes of the synthesized (a, d) HC_4-N_2-CO_2-$Zn(OAC)_2$, (b, e) HC_6-N_3-CO_2-$Zn(NO_3)_2$, (c, f) HC_{10}-N_4-CO_2-$Zn(OAC)_2$ MOFs. Notice: Aperture of MOFs is mainly less than 2 nm (micropore), so we choose the CO_2 isotherm. The temperature of CO_2 isotherm was 195 K. Horvath-Kawazoe (HK) method was used to test the micropores of MOFs.

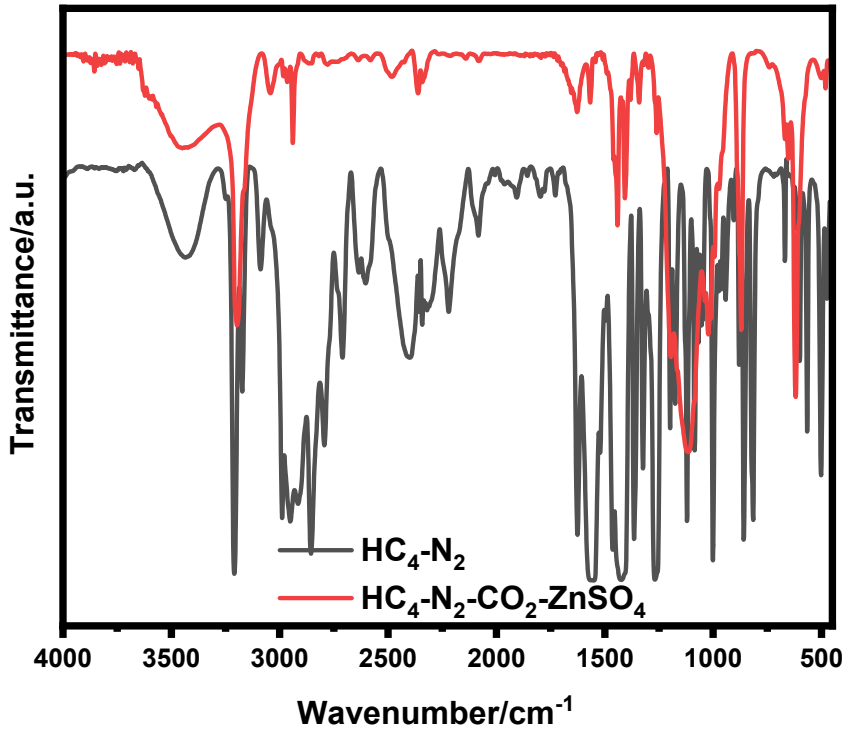

Figure S14. FT-IR spectra of HC_4-N_2 and HC_4-N_2-CO_2-$ZnSO_4$.

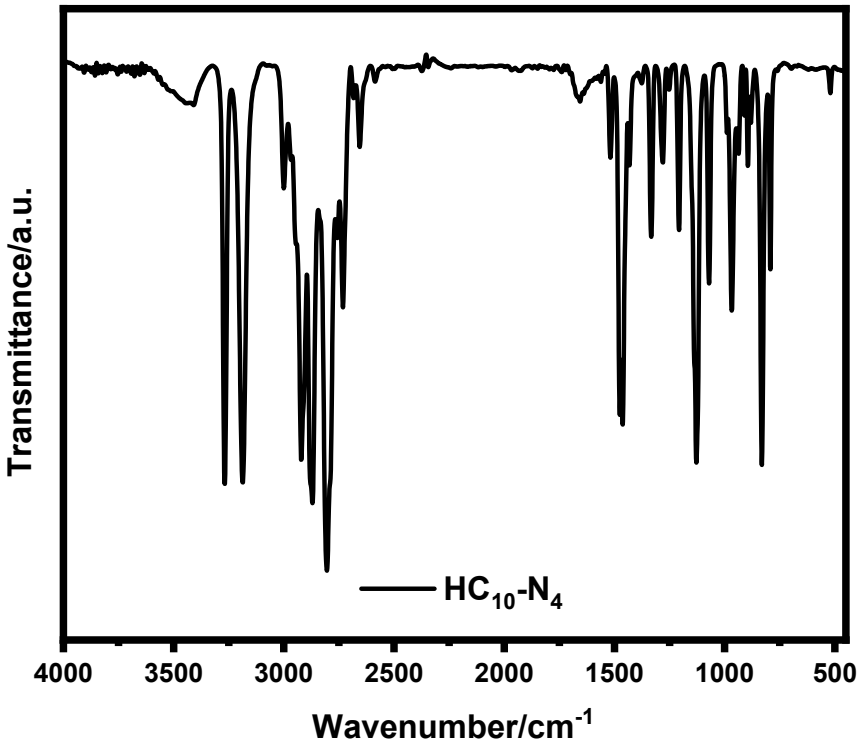

Figure S15. FT-IR spectra of HC_{10}-N_4.

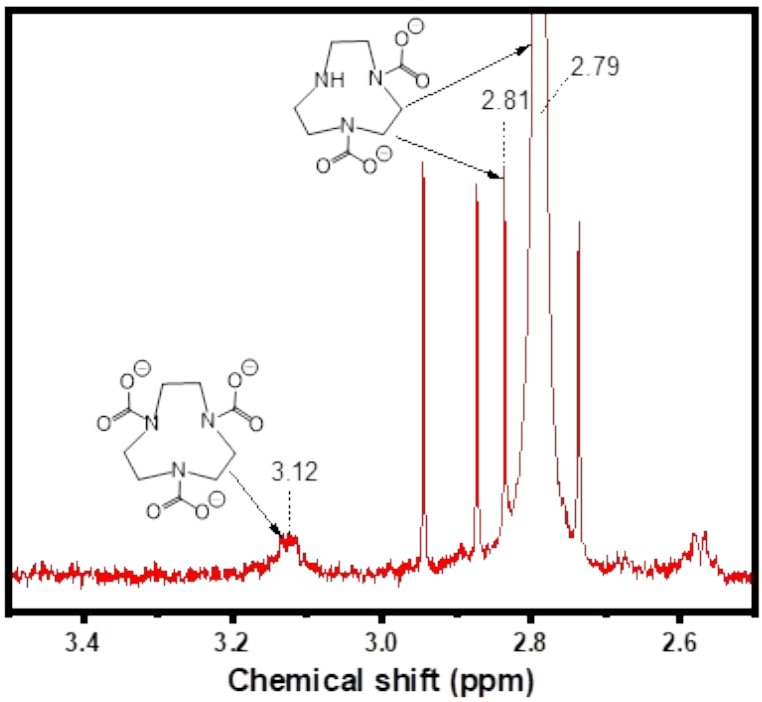

Figure S16. ^{1}H NMR spectrum of HC_6-N_3-CO_2-$Zn(OAC)_2$ dissolved in $CDCl_3$ at T = 298 K.

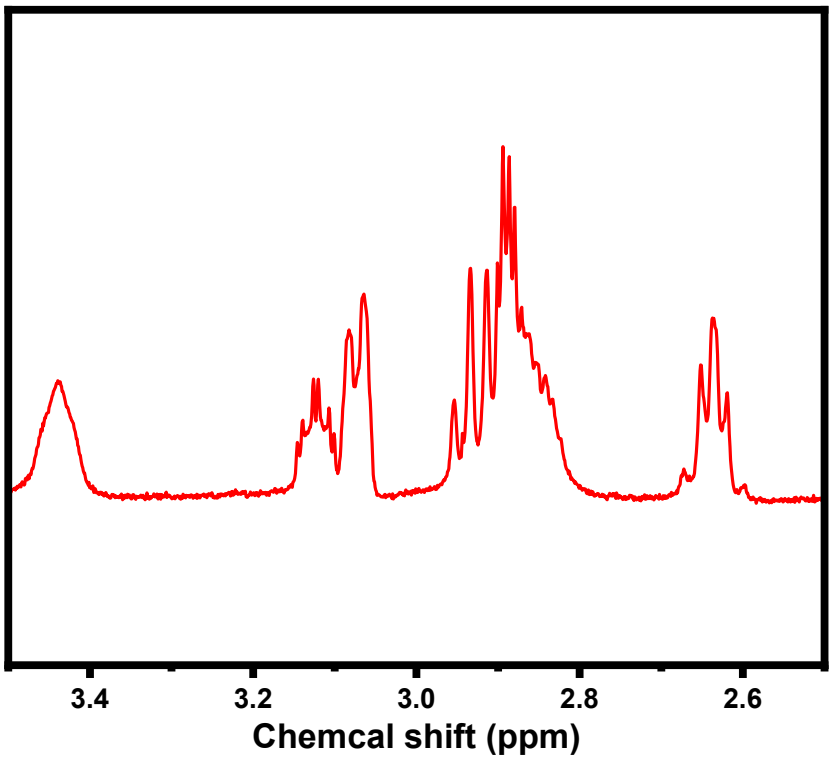

Figure S17. ^{1}H NMR spectrum of HC_{10}-N_4-CO_2-$Zn(OAC)_2$ dissolved in $CDCl_3$ at T = 298 K.

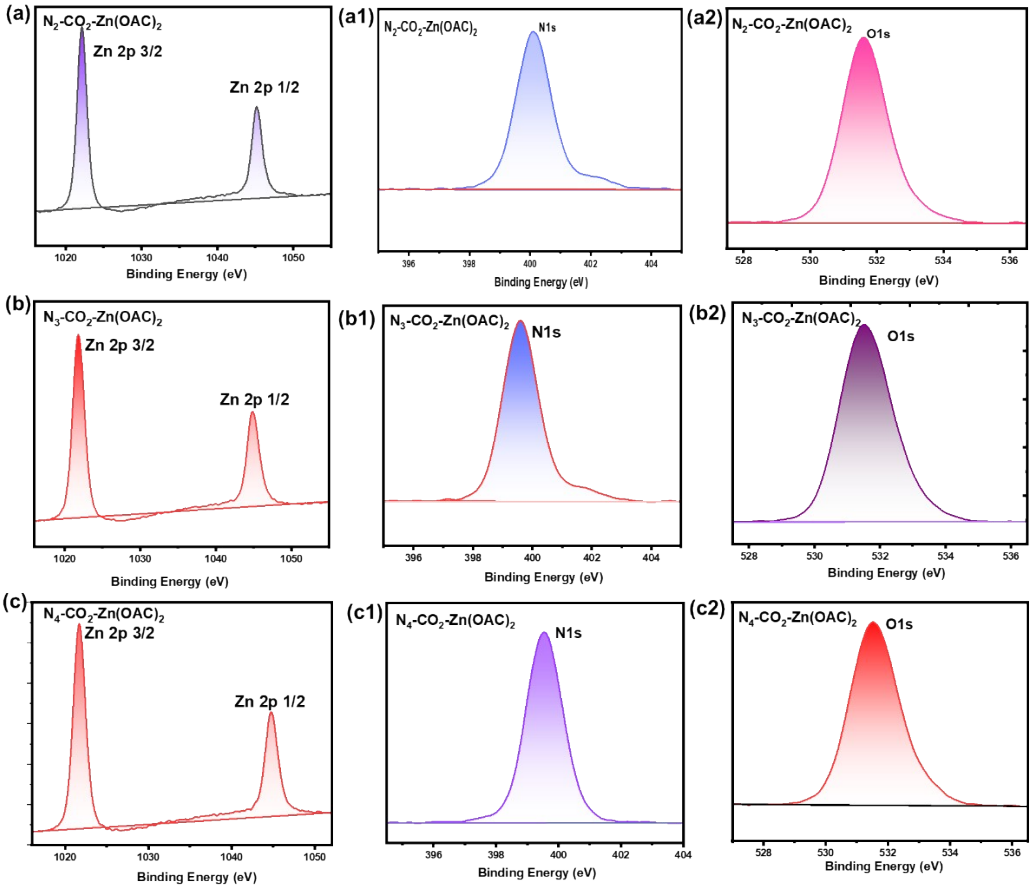

Figure S18. Fine Zn 2p, N 1s, O 1s XPS spectra of different MOFs samples. **a-a2**, HC_4-N_2-CO_2-$Zn(OAC)_2$. **b-b2**, HC_6-N_3-CO_2-$Zn(OAC)_2$.**c-c2**, HC_{10}-N_4-CO_2-$Zn(OAC)_2$.

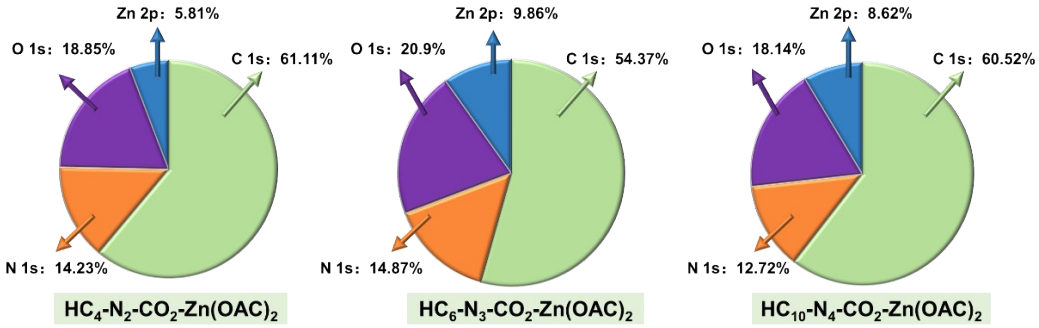

Figure S19. Pie charts of different atomic ratios in different MOFs.

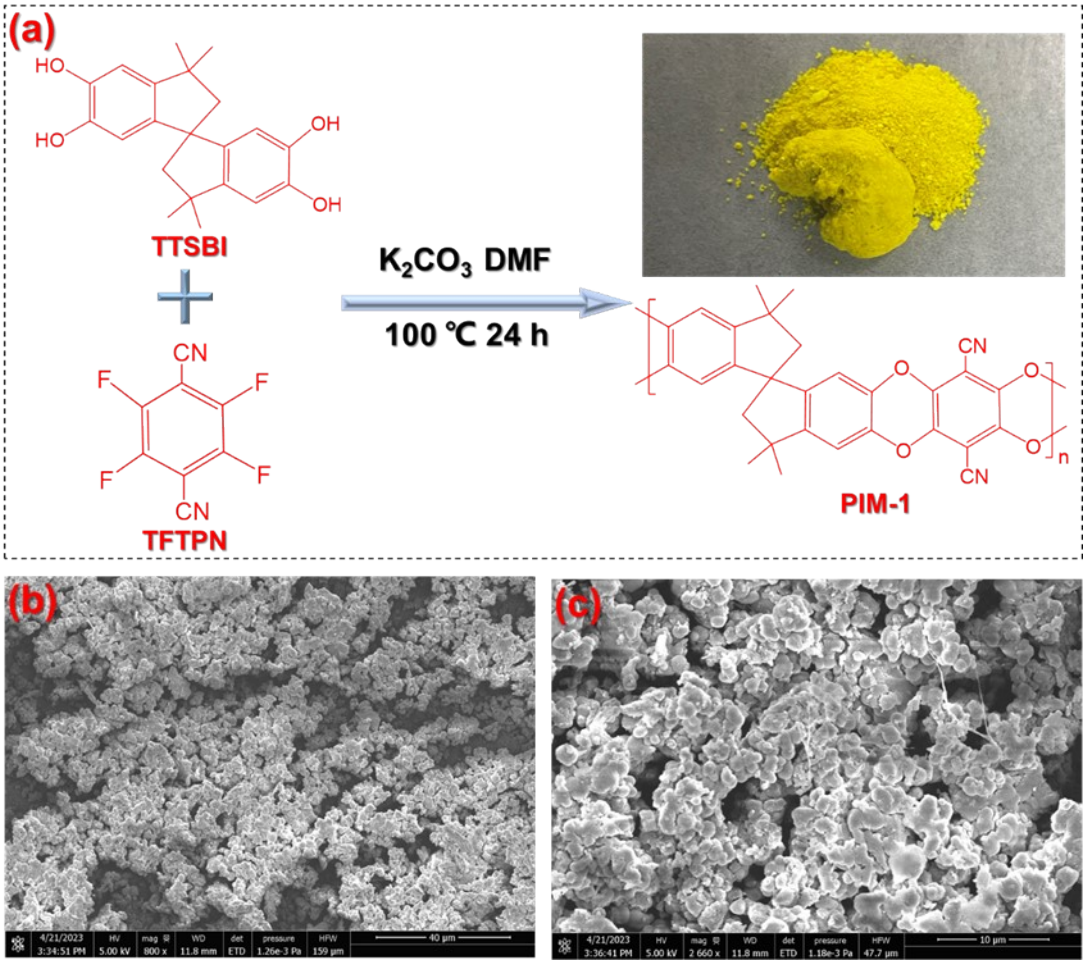

Figure S20. Synthesis and SEM pictures of PIM-1.

TTSBI: 5,5′,6,6′-tetrahydroxy-3,3,3′,3′ tetramethylspirobisindane; TTFPN: 2,3,5,6-tetrafluoroterephthalonitrile; Solvent was dimethylformamide.

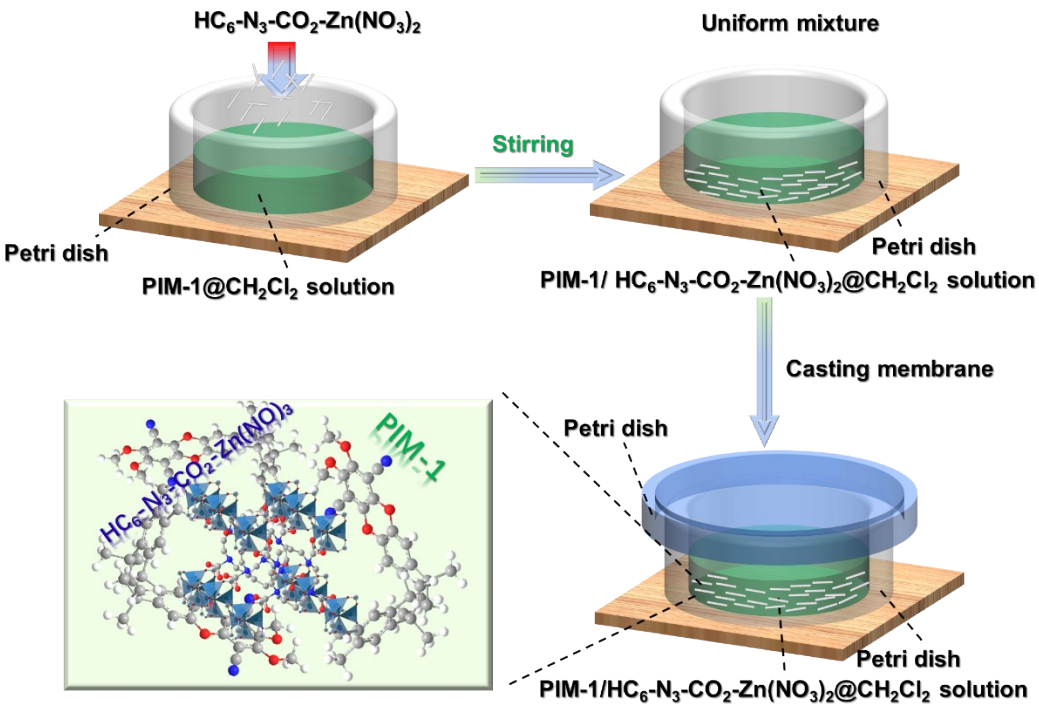

Figure S21 Preparation diagram of PIM-1/HC_6-N_3-CO_2-$Zn(NO_3)_2$ (1%) MMMs

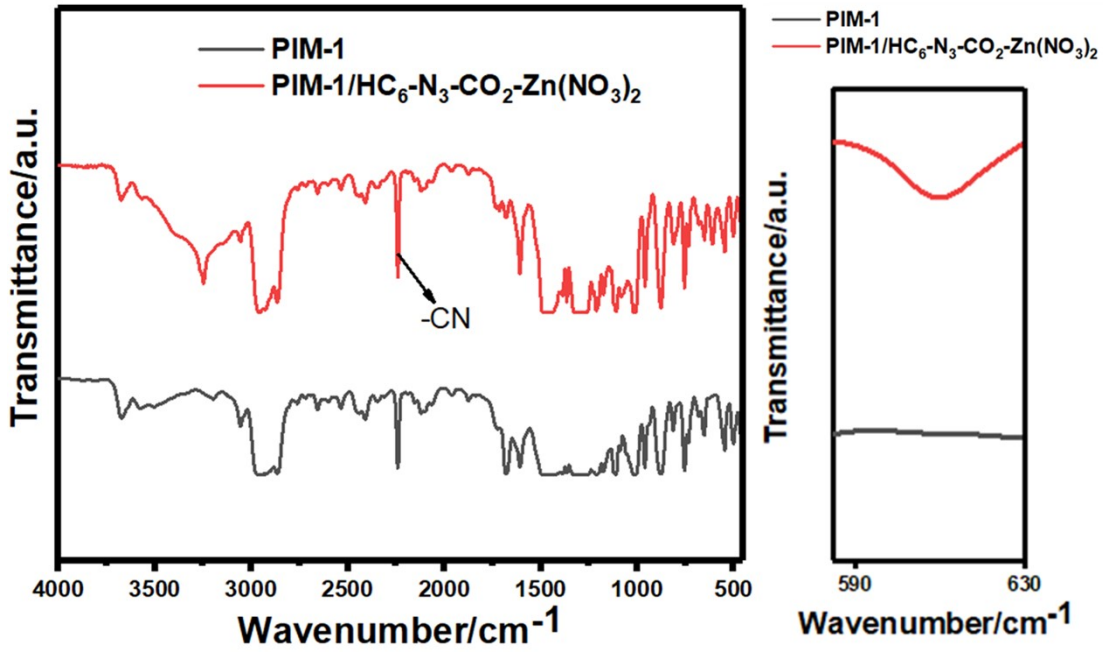

Figure S22. FTIR spectra of the pure PIM-1 and PIM-1/HC_6-N_3-CO_2-$Zn(NO_3)_2$ (1%) MMMs.

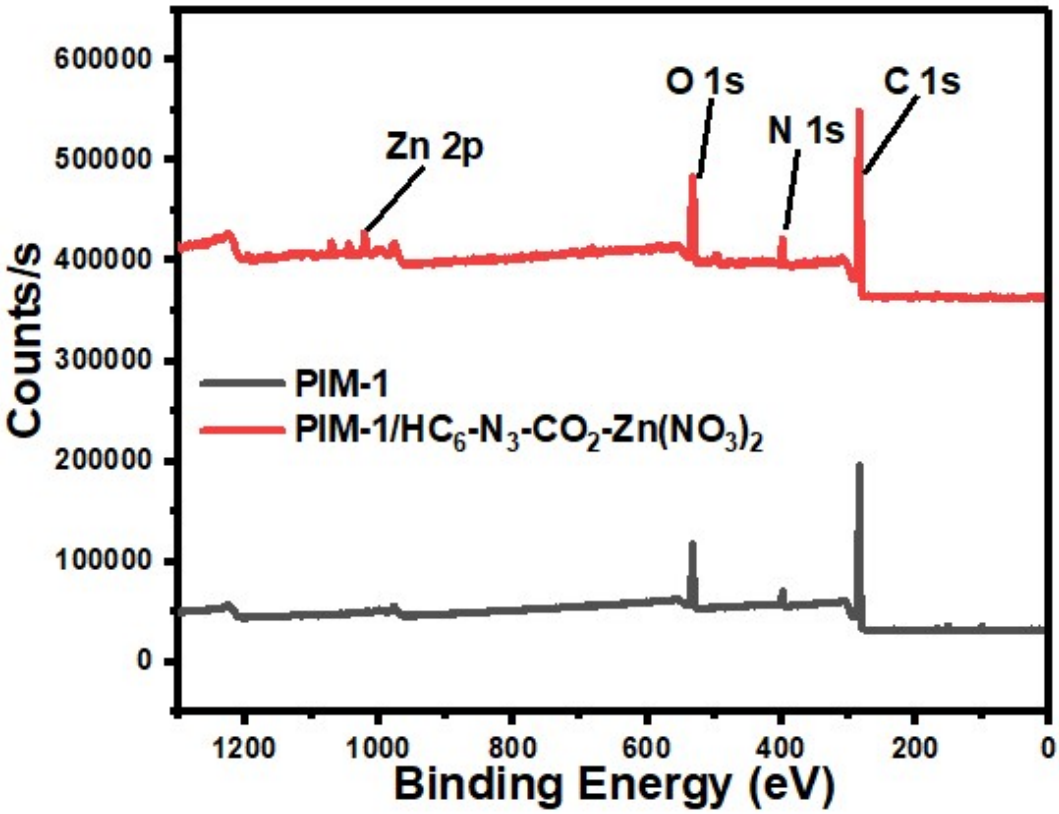

Figure S23. XPS survey spectra of the pure PIM-1 membrane and PIM-1/HC_6-N_3-CO_2-$Zn(NO_3)_2$.

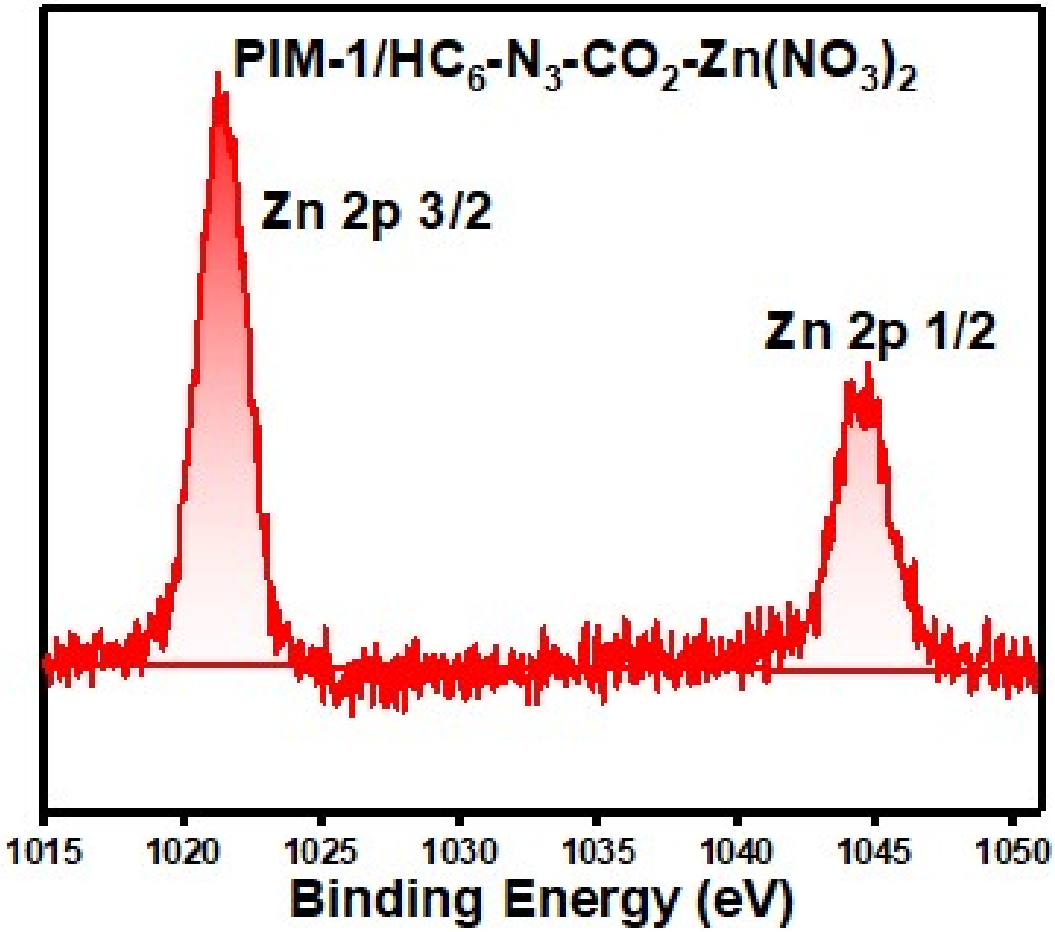

Figure S24. Fine Zn 2p XPS spectra of PIM-1/HC_6-N_3-CO_2-$Zn(NO_3)_2$ (1%) MMMs.

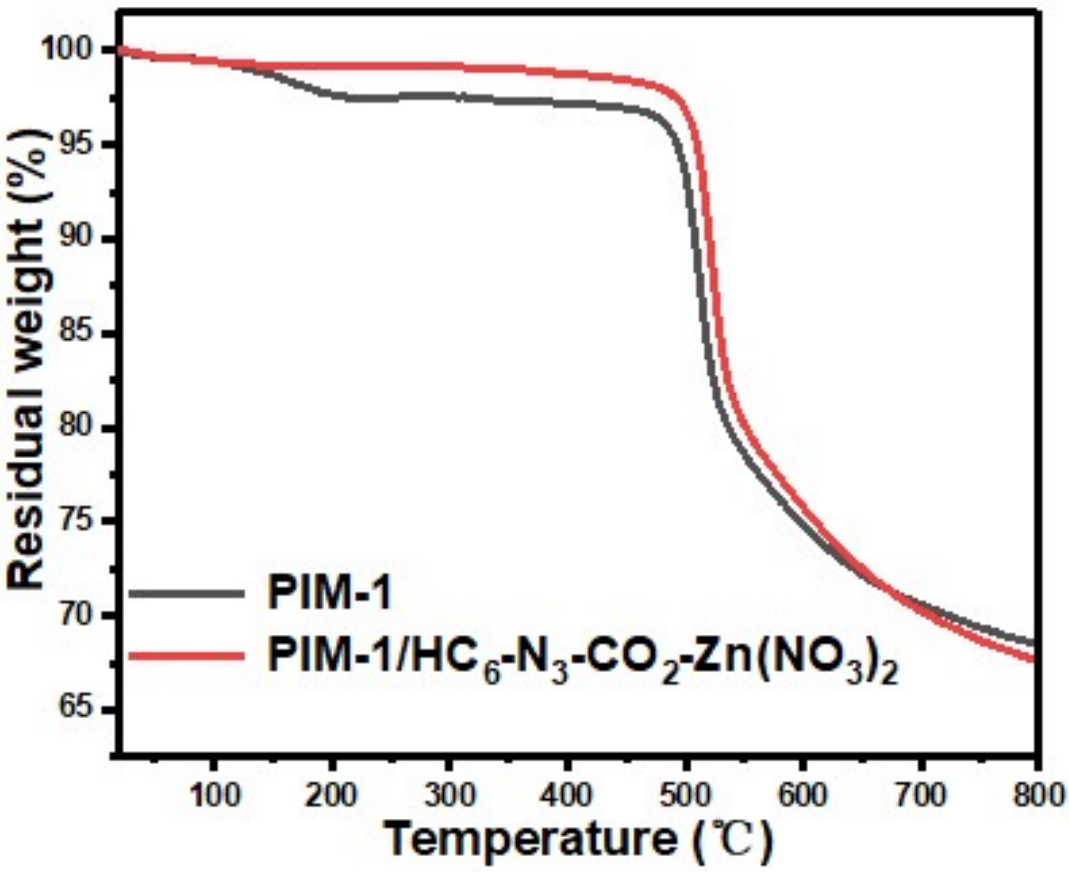

Figure S25. TGA of the pure PIM-1 membrane andPIM-1/HC_6-N_3-CO_2-$Zn(NO_3)_2$ (1%) MMMs.

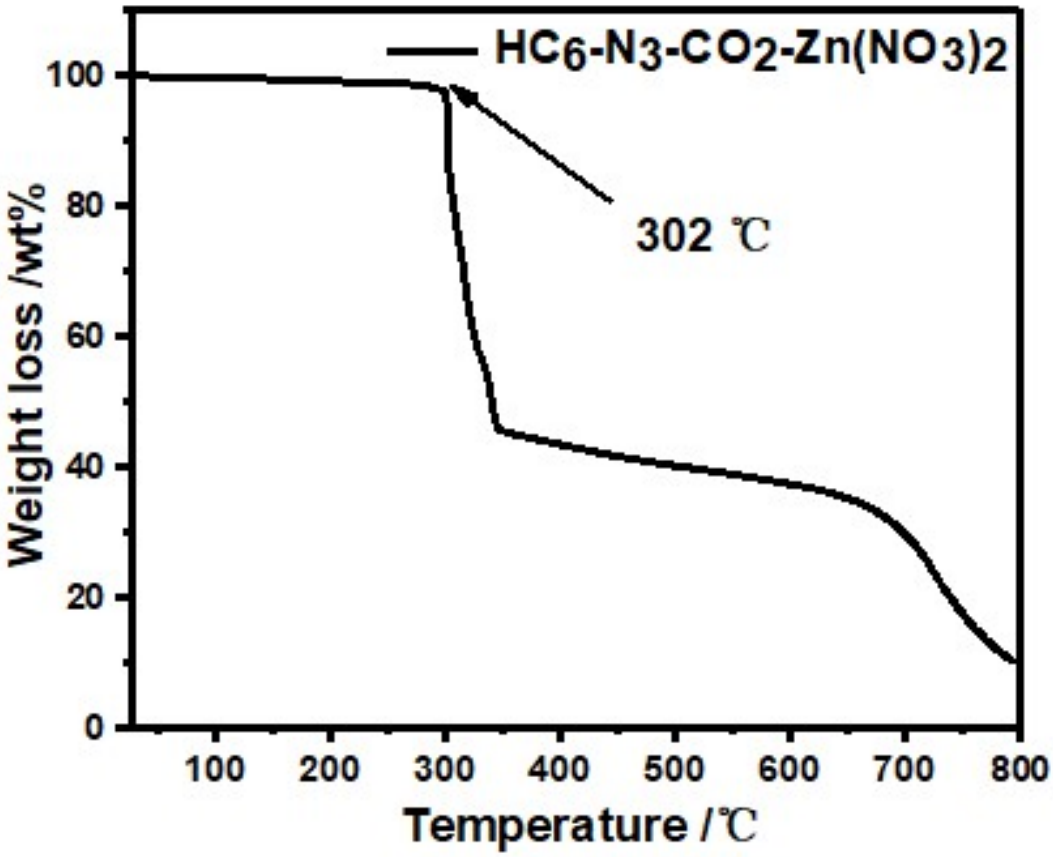

Figure S26 TGA of HC_6-N_3-CO_2-$Zn(NO_3)_2$ powders.

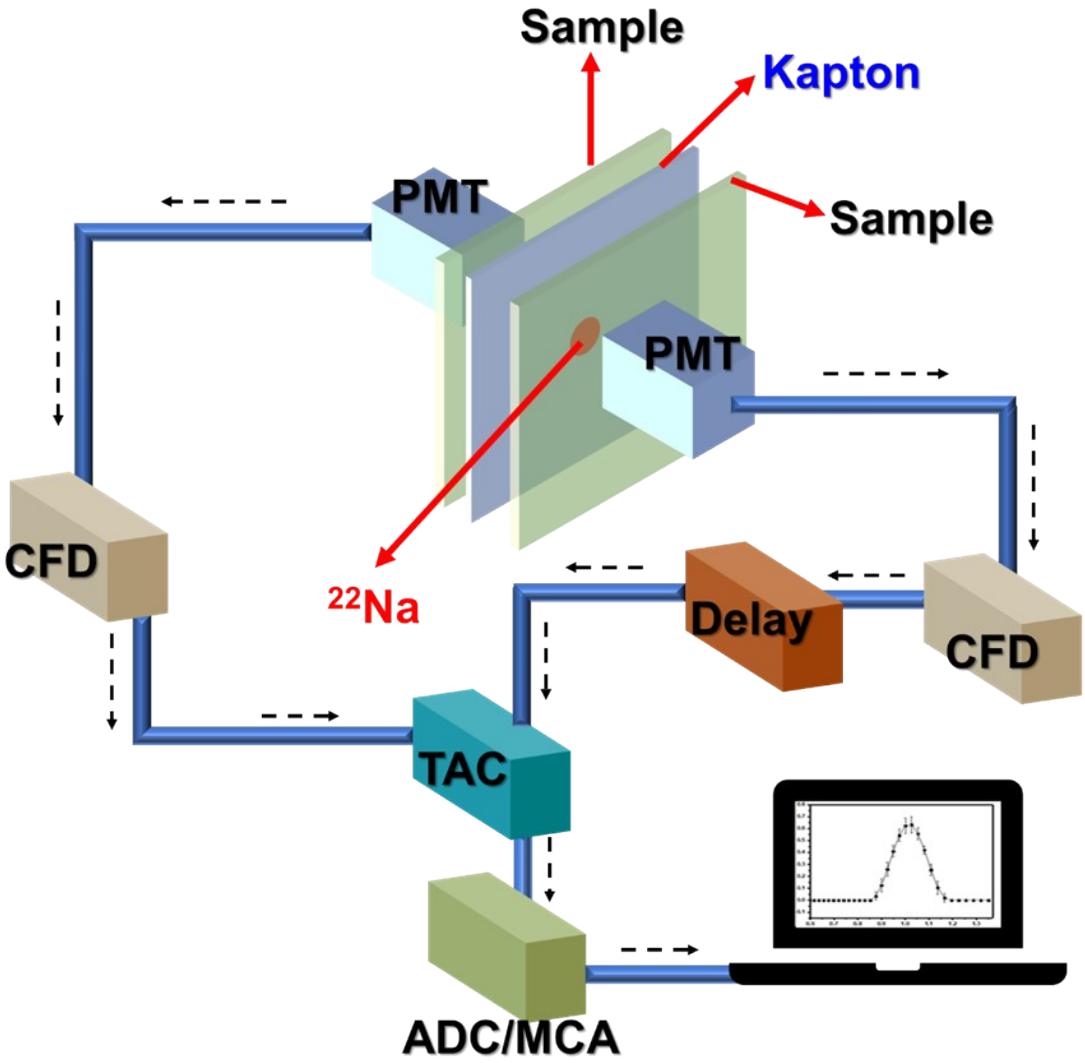

Figure S27. Schematic diagram of positron annihilation lifetime spectroscopy (PALS).

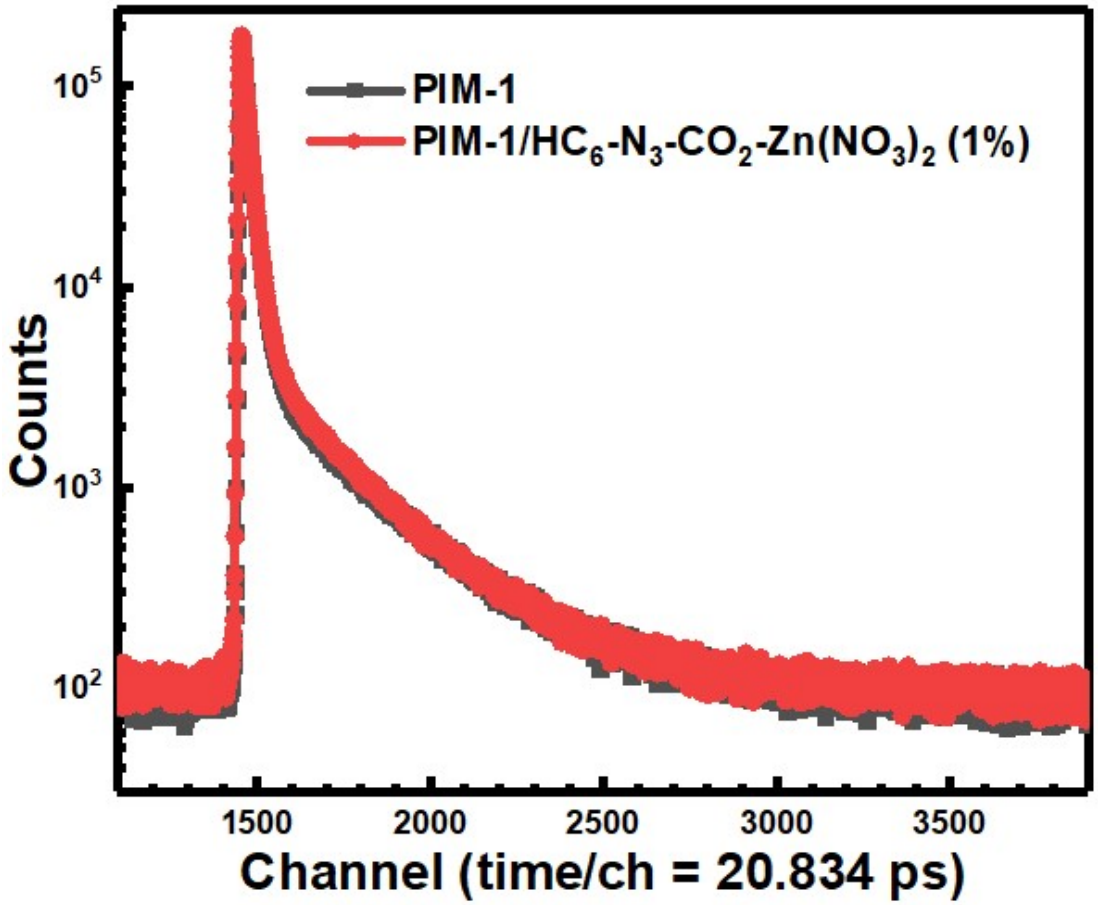

Figure S28. Peak-normalized positron lifetime spectra measured for the PIM-1 and PIM-1/HC_6-N_3-CO_2-$Zn(NO_3)_2$ (1 %) membranes.

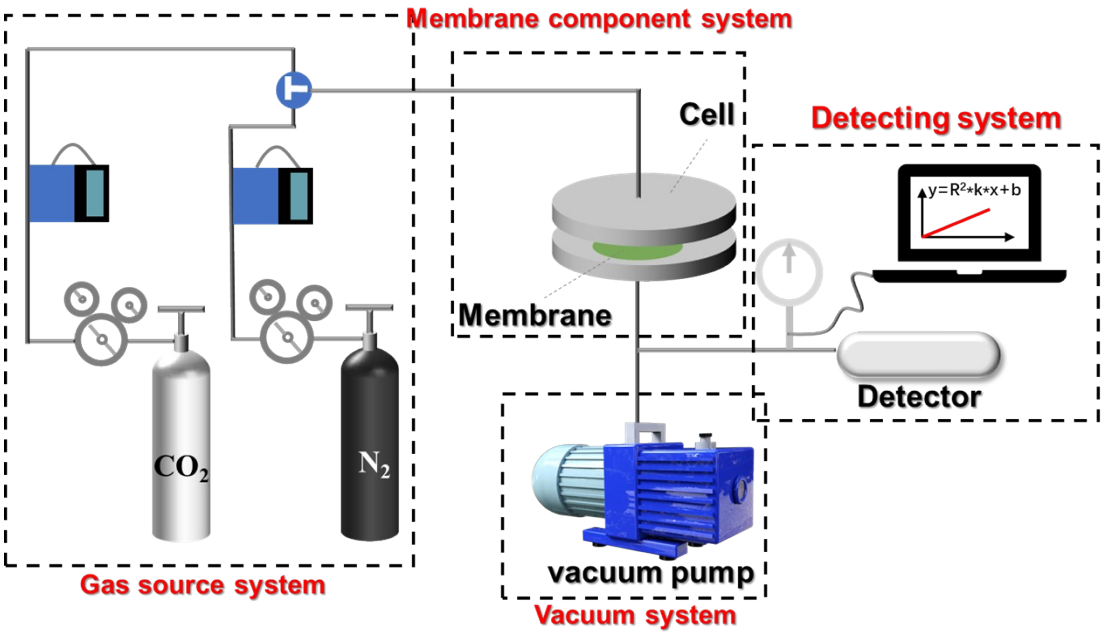

Figure S29. The illustration of the home-made apparatus including gas sources, membrane modules, vacuum and detecting system for gas permeation tests.

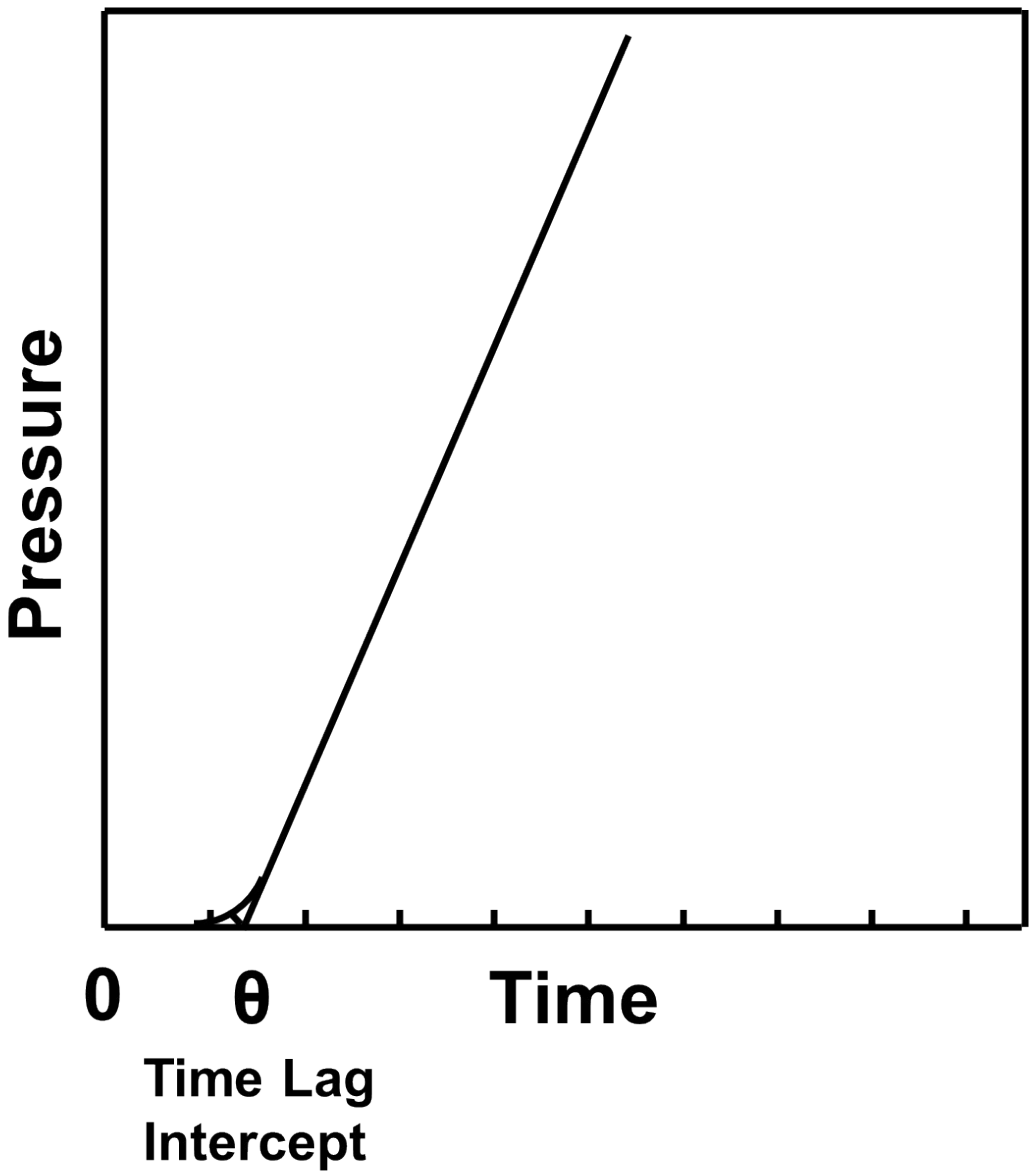

Figure S30. Time-lag derived from the gas permeation curve.

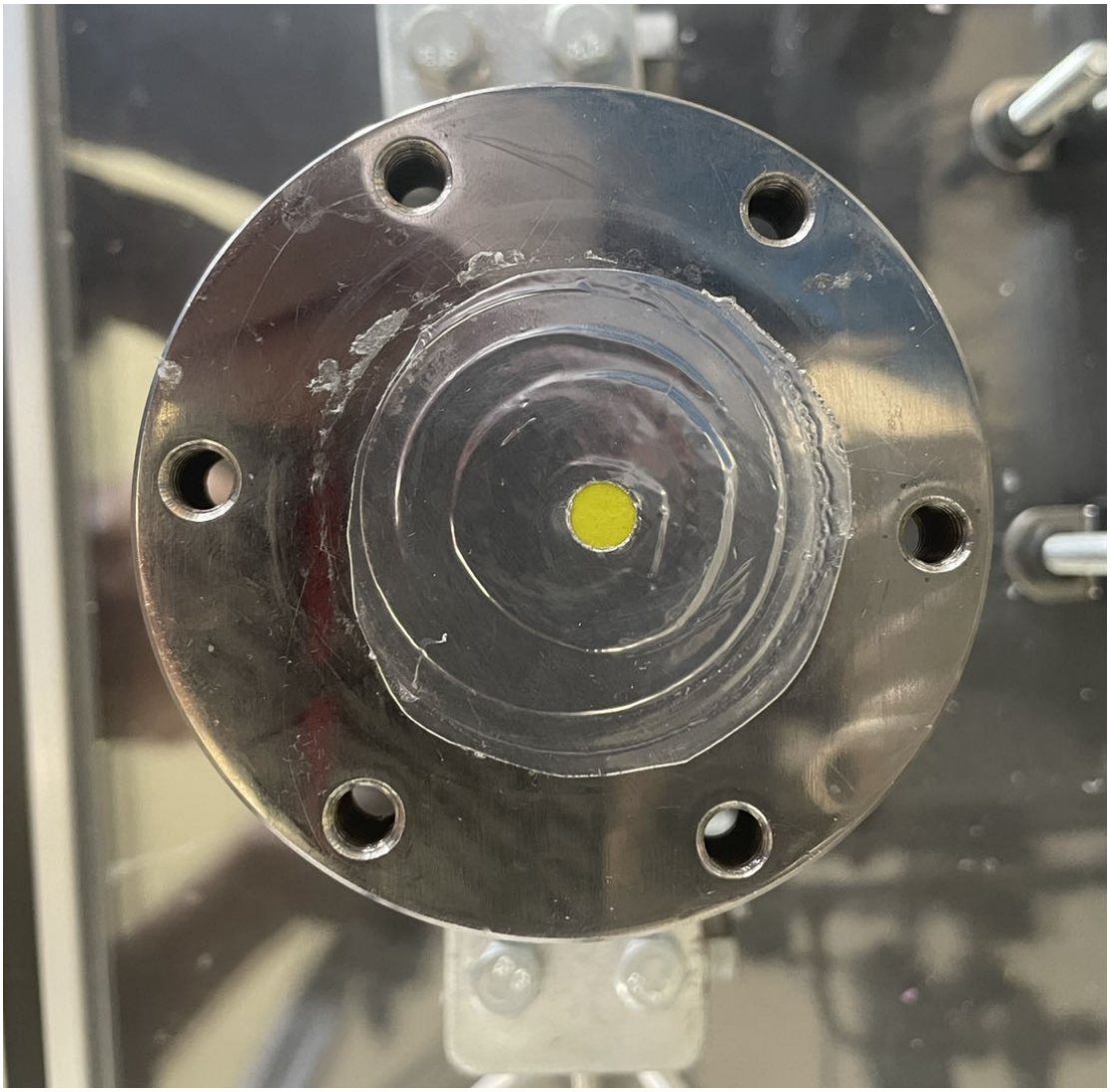

Figure S31. Digital picture of PIM-1/HC_6-N_3-CO_2-$Zn(NO_3)_2$ (1%) MMMs in the cell of the gas permeation apparatus.

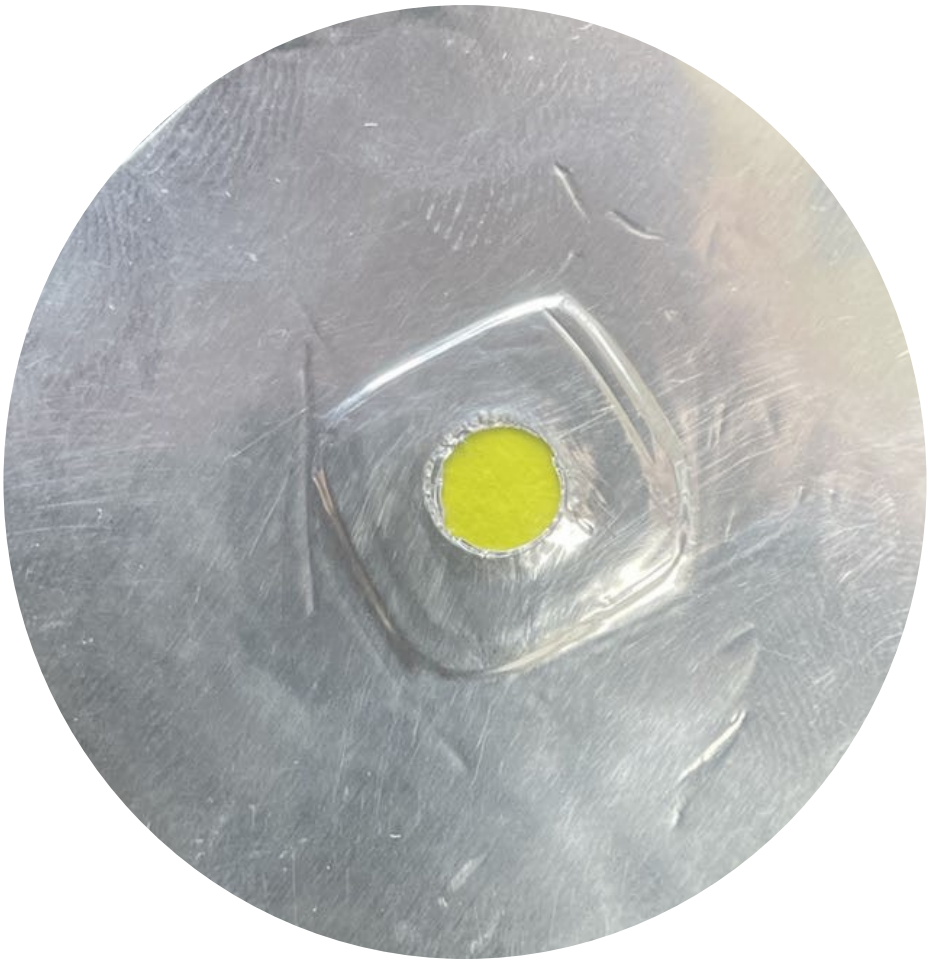

Figure S32. Digital picture of the PIM-1 membrane.

Table S3 PALS results of the PIM-1 and PIM-1/HC_6-N_3-CO_2-$Zn(NO_3)_2$ (1 %) membranes.

Membrane	τ_1 [ns]	τ_2 [ns]	τ_3 [ns]	τ_4 [ns]	I_3 [%]	I_4 [%]	R_3	R_4
PIM-1	0.166 ± 0.0013	0.497± 0.0018	3.21±0 .18	6.55±0 .12	8.25±0 .78	17.7±0 .77	0.381±0. 012	0.552±0. 0049
PIM-1/HC_6-N_3-CO_2-$Zn(NO_3)_2$ （1%）	0.175 ±0.000 7 0	0.486± 0.0013	2.94±0 .11	6.28±0 .091	9.04±0 .50	16.5±0 .52	0.363±0. 0077	0.541±0. 0039

Table S4. Physical parameters of H_2, CO_2, N_2 and CH_4.

Molecule	Kinetic diameter (Å)	Polarizability (10^{-25} cm^{-3})	Dipole moment (10^{-19} esu^{-1} cm^{-1})	Quadrupole moment (10^{-27} esu^{-1} cm^{-1})
H_2	2.89	8.04	0	6.62
CO_2	3.30	29.1	0	43.0
N_2	3.64	17.4	0	15.2
CH_4	3.76	25.93	0	0

Table S5 Gas permeability and selectivity of PIM-1/HC_6-N_3-CO_2-$Zn(NO_3)_2$（1 %）MMMs at 2 bar and 298 K

Membranes	Permeability (Barrer)				Selectivity		
	H_2	CO_2	N_2	CH_4	CO_2/N_2	CO_2/CH_4	H_2/N_2
PIM-1	2566±22	3898±36	171±3	210±3	22±0.58	18±0.15	15±0.12
PIM-1/HC_6-N_3-CO_2-$Zn(NO_3)_2$ (1 %)	5066±50	13343±520	686±5	700±1	20±0.32	19±0.19	7±0.13

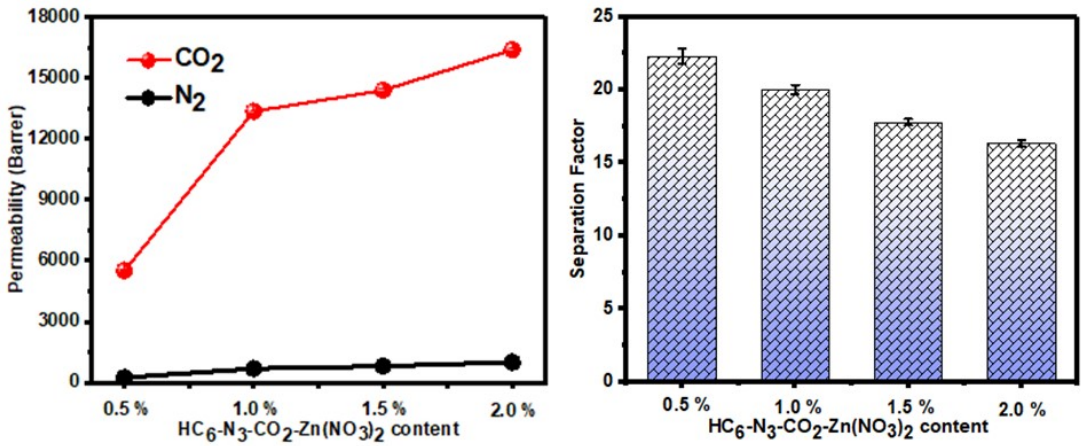

Figure S33. (a) CO_2 and N_2 permeability, (b) the selectivity of CO_2/N_2 of MMMs under different HC_6-N_3-CO_2-$Zn(NO_3)_2$ loading (0.5 wt%, 1.0 wt%, 1.5 wt%, 2.0 wt%).

Table S6 Gas permeability and selectivity of PIM-1/HC_6-N_3-CO_2-$Zn(NO_3)_2$ (1%) MMMs at 2 bar and 298 K during long-term tests.

Time (h)	Permeability (Barrer)		Selectivity
	CO_2	N_2	CO_2/N_2
0	13343±520	601±64	20.02±0.32
12	10925±516	589±35	18.08±1.17
18	10860±526	583±32	18.08±1.07
24	10467±532	580±34	17.76±0.82
36	10568±422	556±23	18.14±0.86
48	10681±462	551±24	18.42±0.75
60	9928±450	546±26	17.85±0.67
66	9758±396	537±25	17.70±0.75
72	10058±385	504±26	18.42±0.56
96	9569±366	483±25	17.82±0.11
108	9822±371	423±26	19.50±0.23
120	9354±322	391±25	19.36±0.31
144	9060±316	365±21	21.43±0.71
168	8784±268	583±19	22.48±0.55
192	9264±296	580±26	25.41±0.67

Table S7 Gas permeability and selectivity of PIM-1/HC_6-N_3-CO_2-$Zn(NO_3)_2$ (1 %) MMMs at 298 K and different pressures

Pressures (bars)	Permeability (Barrer)	Selectivity
	CO_2	CO_2/N_2
1	11602±537	20±0.83
3	10229±516	12±0.66
5	9727±427	16±0.52
3	10475±502	18±0.62
1	125095±565	21±0.71
3	93425±486	22±0.75
5	8648±362	18±0.41
3	86428±381	21±0.53
1	99688±392	21±0.58

Table S8 Comparison of CO_2 permeability and CO_2/gases selectivity between PIM-1/HC_6-N_3-CO_2-$Zn(NO_3)_2$ (1 %) MMMs in this work and other reported PIM-1/MOF MMMs.

Polymer	MOF	Loading (wt.%)	Measurement conditions	CO_2 Permeability (Barrer)	CO_2/N_2 Selectivity	CO_2/CH_4 Selectivity	Ref.
PIM-1	HZIF-8	16.7	3.5 bar, 308 K	8268	25.1	18.7	[S24]
PIM-1	ZIF-8	67.2	3.5 bar, 308 K	6338	24.4	18.8	[S25]
PIM-1	UiO-66-NH_2	10	4 bar, 298 K	2869	27.5	28.3	[S26]
PIM-1	UiO-66-CN	20	1.4 bar, 298 k	7070.9	26.7	-	[S27]
PIM-1	IL-UiO	20	2 bar, 298 K	13778		35.2	[S28]
Matrimid	UiO-66	11	-	22	33.5	-	[S29]
Matrimid	MMIF	20	4 bar, 308 K	8.65	27.0	34.6	[S30]
Matrimid	Cu(BDC)	4	-	6.4	42	-	[S31]
Matrimid	UiO-66-NH_2@ICA	10	3 bar, 298 K	41	64.2	-	[S32]
Matrimid	ZiF-78	20	5 bar, 308 k	24	29	-	[S33]
Matrimid	ZiF-95	30	3 bar, 303 k	23.2	-	58	[S34]
Matrimid	MOF-5	-	2 bar, 308 k	20.2	38.8	-	[S35]
polyimide	ZiF-90	15	2 bar, 298 K	720	-	37	[S36]
polyimide	PI/IPD@ZIF-8	45	3 bar, 308 K	4133	6.8	7.8	[S37]
polyimide	(CBMNs	2	3 bar, 298 K	368	-	33.6	[S38]
polyimide	GO (30)_UiO-66	32	308 k	21	-	51	[S39]
Polyimide	ZIF-11	20	4 bar, 303 K	258	-	31	[S40]
PIM-1/HC_6-N_3-CO_2-$Zn(NO_3)_2$(1 %)	HC_6-N_3-CO_2-$Zn(NO_3)_2$	1	2 bar, 298 K	13343	20	19	This work

PIM-1/HC_6-N_3-CO_2-$Zn(NO_3)_2$(1 %, Aging192 h)	HC_6-N_3-CO_2-$Zn(NO_3)_2$	1	2 bar, 298 K	9264	25.5	-	This work

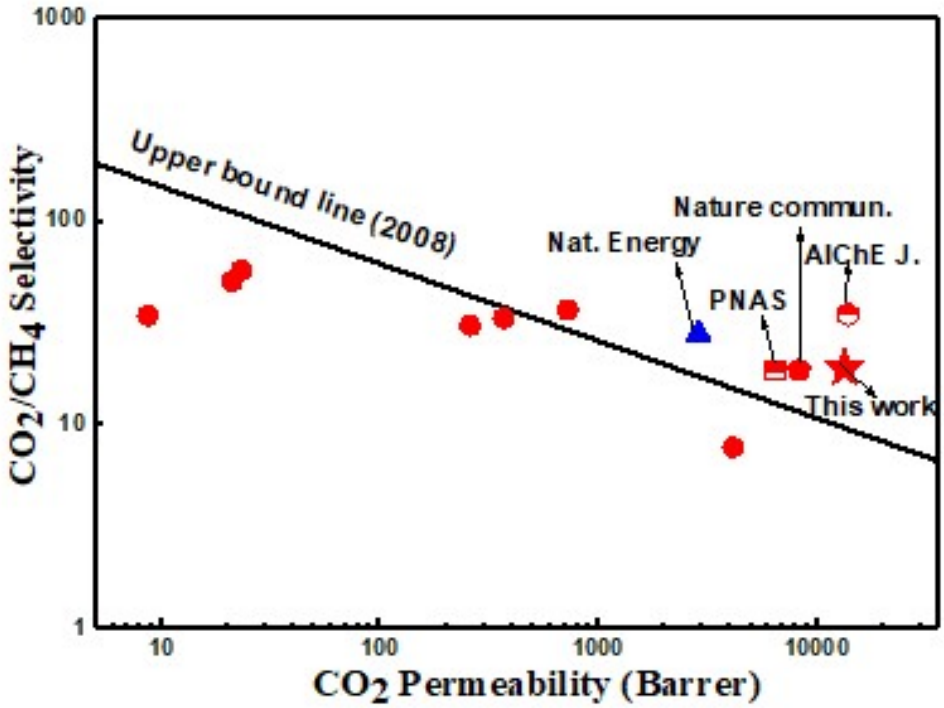

Figure S34. Selectivity versus permeability for CO_2/CH_4, where gas separation performance of the MMMs prepared in this work (pentacles) and various MOF-based MMMs from literatures plotted against the Robeson plot of 2008. A fully detailed comparison of the data in this plot could be found in the Table S7.

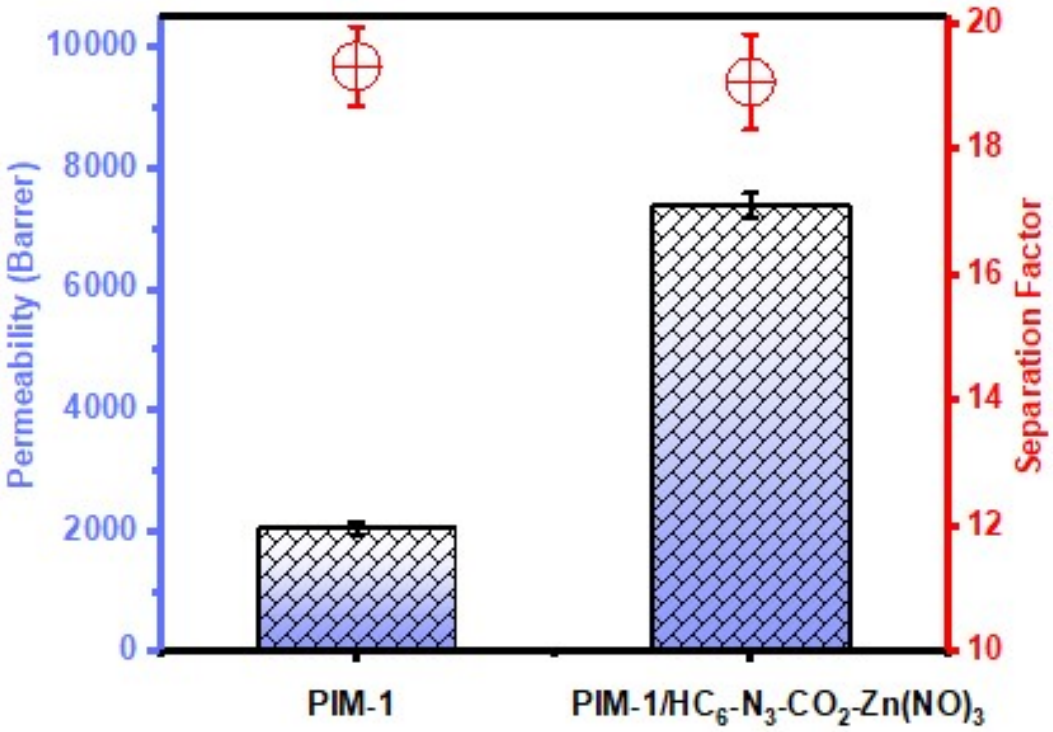

Figure S35. Binary CO_2/N_2 (50/50) mixed-gas performance of PIM-1 and PIM-1/HC_6-N_3-CO_2-$Zn(NO_3)_2$ (1%) membranes.

Video S1 Absorbing Exhaled CO_2 by HC_4-N_2. A phase transition process occurs rapidly.

Video S2 Long duration (12 h) for CO_2 absorption with high efficiency.

Supplementary References

[S1] K. Kadota *et al.,* One-pot, room-temperature conversion of CO_2 into porous metal-organic frameworks. *J. Am. Chem. Soc.* **143**, 16750-16757 (2021).

[S2] K. Kadota, N. T. Duong, Y. Nishiyama, E. Sivaniah, S. Horike, Synthesis of porous coordination polymers using carbon dioxide as a direct source. *Chem. Commun.* **55**, 9283-9286 (2019).

[S3] E. J. Kim, R. L. Siegelman, H. Z. H. Jiang, A. C. Forse, J. H. Lee, J. D. Martell1, P. J. Milner, J. M. Falkowski, J. B. Neaton, J. A. Reimer, S. C. Weston, J. R. Long, *Science* **2020**, *369*, 392-396.

[S4] K. Sumida, D. L. Rogow, J. A. Mason, T. M. McDonald, E. D. Bloch, Z. R. Herm, T. Bae, J. R. Long, *Chem. Rev.* **2012**, *11*, 724-781.

[S5] J. B. Lin, T. T. T. Nguyen, R. Vaidhyanathan, J. Burner, J. M. Taylor, H. Durekova, F. Akhtar, R. K. Mah, O. Ghaffari-Nik, S. Marx, N. Fylstra, S. S. Iremonger, K. W. Dawson, P. Sarkar, P. Hovington, A. Rajendran, T. K. Woo, G. K. H. Shimizu, *Science* **2021**, *374*, 1464.

[S6] M. Gholami, B. Verougstraete, R. Vanoudenhoven, G. V. Baron, T. V. Assche, J. F. Denayer, *Chem. Eng. J.* **2022**, *43*, 133380.

[S7] H. J. Choi, S. B. Hong, *Chem. Eng. J.* **2022**, *433*, 13380.

[S8] S. Wang, S. M. Mahurin, S. Dai, D. *ACS Appl. Mater. Interfaces* **2021**, *13*, 17511-17516.

[S99] L. P. Silva, E. A. Crespo, M. A. R. Martins, P. C. Barbosa, R. L. Gardas, L. F. Vega, J. A. P. Coutinho, P. J. Carvalho, *Ind. Eng. Chem. Res.* **2022**, *61*, 4046-4057.

[S10] Y. He, X. Li, W. Cai, H. Lu, J. Ding, H. Li, H. Wan, G. Guan, *ACS Sustainable Chem. Eng.* **2021**, *9*, 7074-7085.

[S11] Y. Liu, Q. Ye, M. Shen, J. Shi, J. Chen, H. Pan, Y. Shi, *Environ. Sci. Technol.* **2011**, *45*, 5710-5716.

[S12] C. Zhou, S. Yu, K. Ma, B. Liang, S. Tang, C. Liu, H. Yue, *Chem. Eng. J.* **2021**, *413*, 127675.

[S13] M. S. Yeganeh, A. Jusufi, S. P. Deighton, M. S. Ide, M. Siskin, A. Jaishankar, C. Maldarelli, P. Bertolini, B. Natarajan, J. L. Vreeland, M. A. King, A. R. Konicek, *Sci. Adv.* **2022**, *8*, eabm0144.

[S14] H. Stephan, S. Linus, O. Hyunchul, H. Michael, V. L. Bettina, *Chem. Mater.* **2015** *27*, 8001-8010.

[S15] X. Zhu, C. Tian, G. M. Veith, C. W. Abney, J. Dehaudt, S. Dai, *J. Am. Chem. Soc.* **2016**, *138*, 11497-11500.

[S16] S. Kikkawa, K. Amamoto, Y. Fujiki, J. Hirayama, G. Kato, H. Miura, T. Shishido, S. Yamazoe, *ACS Environ. Au* **2022**, *2*, 354.

[S17] S. Bureekaew, S. Shimomura, S. Kitagawa, *Sci. Technol. Adv. Mater.* **2008**, *9*, 1-12.

[S18] S. Kikkawa *et al.,* Direct air capture of CO_2 using a liquid amine-solid carbamic acid phase-separation system using diamines bearing an aminocyclohexyl group. *ACS Environ. Au* **2**, 354-362 (2022).

[S19] Y. Qiu et al., Phase-change CO_2 absorption using novel 3-dimethylaminopropylamine with primary and tertiary amino groups. *Ind. Eng. Chem. Res.* **59**, 8902-8910 (2020).

[S20] X. Xu *et al.,* Next generation amino acid technology for CO_2 capture. *J. Mater. Chem. A* **9**, 1692 (2021).

[S21] C. María, G. D. Diego, M. N. José, Carbon dioxide chemical absorption using methyl piperidines aqueous solutions. *Fuel* **197**, 194-200 (2017).

[S22] M. M. Sergey, S. Matthias, Molecular dynamics study of the solution structure, clustering, and diffusion of four aqueous alkanolamines. *J. Phys. Chem. B* **122**, 2769-2778 (2018).

[S23] B. Liu, X. Luo, Z. W. Liang, O. Wilfred, H. Liu, The development of kinetics model for CO_2 absorption into tertiary amines containing carbonic anhydrase. *AIChE J.* **63**, 4933-4943 (2017).

[S24] B. Zhu *et al.,* Boosting membrane carbon capture via multifaceted polyphenol-mediated soldering. *Nat. Commun.* **14**, 1697 (2023)

[S25] S. He *et al.,* Symbiosis-inspired de novo synthesis of ultrahigh MOF growth mixed matrix membranes for sustainable carbon capture. *PANS* **119**, e2114964119 (2022).

[S26] B. Ghalei *et al.,* Enhanced selectivity in mixed matrix membranes for CO_2 capture through e cient dispersion of amine-functionalized MOF nanoparticles. *Nat. energy* **2**, 17086 (2017).

[S27] G. Yu *et al.*, Constructing connected paths between UiO-66 and PIM-1 to improve membrane CO_2 separation with crystal-like gas selectivity. *Adv. Mater.* **31**, 1806 (2019).

[S28] C. Geng, Y. Sun, Z. Zhang, Z.a Qiao, C. Zhong. Mixed matrix metal-organic framework membranes for efficient CO_2/N_2 separation under humid conditions. *AIChE J.* **69**, e18025 (2023).

[S29] A. M. Marti, S. R. Venna, E. A. Roth, J. T. Culp, D. P. Hopkinson. Simple fabrication method for mixed matrix membranes with in situ MOF growth for gas separation. *ACS Appl. Mater. Interfaces* **10**, 24784-24790 (2018).

[S30] M.Ahmadi *et al.,* Highly CO_2 selective microporous metal-imidazolate framework based mixed matrix membranes. *ACS Appl. Mater. Interfaces* **9**, 35936-35946 (2017).

[S31] M. Shete *et al.,* On the direct synthesis of Cu(BDC) MOF nanosheets and their performance in mixed matrix membranes. *J. Membrane Sci.* **549**, 312-320 (2018).

[S32] Y. Jiang, C. Liua, J. Caro, A. Huang. A new UiO-66-NH_2 based mixed-matrix membranes with high CO_2/CH_4 separation performance. *Micropor. Mesopor. Mat.* **274**, 203 (2019).

[S33] M. van Essen, L. van den Akker, R. Thür, M. Houben, I. F. J. Vankelecom, Z. Borneman, K. Nijmeijer, *Adv. Mater. Interfaces* 2021, 8, 2001478.

S34] I. Ilicak, M. S. Boroglu, A. Durmus, I. Boz, J. Nat. Gas Sci. Eng. 2021, 91, 103941.

[S35] E. V. Perez, K. J. Balkus, J. P. Ferraris, I. H. Musselman, Mixed-matrix membranes containing MOF-5 for gas separations. *J. Membrane Sci.* **328**, 165-173 (2009).

[S36] T. H. Bae *et al.,* A High-performance gas-separation membrane containing sub micrometer-sized metal-organic framework crystals. *Angew. Chem. Int. Ed.* **49**, 9863-9866 (2010)

[S37] Y. Shi *et al.,* Mixed matrix membranes with highly dispersed MOF nanoparticles for improved gas separation. *Sep. Purif. Technol.* **277**,119449 (2021).

[S38] X. Bi, MOF Nanosheet-based mixed matrix membranes with metal-organic coordination interfacial interaction for gas separation. *ACS Appl. Mater. Interfaces* **12**, 49101-49110 (2020).

[S39] S Castarlenas, C. Téllez, J. Coronas, Gas separation with mixed matrix membranes obtained from MOF UiO-66-graphite oxide hybrids. *J. Membrane Sci.* **526**, 205-211 (2017).

[S40] M. S. Boroglu, A. B. Yumru. Gas separation performance of 6FDA-DAM-ZIF-11 mixed-matrix membranes for H_2/CH_4 and CO_2/CH_4 separation. S*ep. Purif. Technol.* **173**, 269-279 (2017).